Photos: DOI: 10.1051/ogst/2013204, IFPEN, X.

Dossier

This paper is a part of the hereunder thematic dossier published in OGST Journal, Vol. 69, No. 4, pp. 507-766 and available online here

Cet article fait partie du dossier thématique ci-dessous publié dans la revue OGST, Vol. 69, n°4 pp. 507-766 et téléchargeable ici

DOSSIER Edited by/Sous la direction de : **Z. Benjelloun-Touimi**

Geosciences Numerical Methods
Modélisation numérique en géosciences

Oil & Gas Science and Technology – Rev. IFP Energies nouvelles, Vol. 69 (2014), No. 4, pp. 507-766

IFP Energies nouvelles

Oil & Gas Science and Technology – Rev. IFP Energies nouvelles, Vol. 69 (2014), No. 4, pp. 701-729

DOI: 10.2516/ogst/2013158

Dossier

Geosciences Numerical Methods
Modélisation numérique en géosciences

A Review of Recent Advances in Discretization Methods, *a Posteriori* Error Analysis, and Adaptive Algorithms for Numerical Modeling in Geosciences

Daniele A. Di Pietro[1]* and Martin Vohralík[2]

[1] *Université de Montpellier 2, I3M, 34057 Montpellier Cedex 5 - France*
[2] *INRIA Paris-Rocquencourt, BP 105, 78153 Le Chesnay - France*
e-mail: daniele.di-pietro@univ-montp2.fr - martin.vohralik@inria.fr

* Corresponding author

Résumé — **Une revue des avancées récentes autour des méthodes de discrétisation, de l'analyse *a posteriori*, et des algorithmes adaptatifs pour la modélisation numérique en géosciences** — Cet article de revue traite de deux thématiques de recherche en géosciences qui ont connu d'importants développements au cours des dernières années. Dans la première partie, on considère un ingrédient clé pour la résolution numérique du problème d'écoulement de Darcy, à savoir les schémas de discrétisation des termes de diffusion sur des maillages polygonaux/polyédriques généraux. On présente différents schémas et on discute en détail de leurs propriétés numériques fondamentales telles que la stabilité, la consistance et la robustesse. La deuxième partie de l'article est consacrée au contrôle de l'erreur et à l'adaptivité pour des problèmes modèles en géosciences. On présente des estimations *a posteriori* qui garantissent une borne supérieure de l'erreur totale et qui permettent d'identifier les différentes composantes d'erreur. Ces estimations sont utilisées pour formuler des critères d'arrêt adaptatifs pour des solveurs linéaires et non linéaires ainsi que pour ajuster le pas de temps et pour raffiner le maillage de façon adaptative. Des essais numériques illustrent le caractère entièrement adaptatif de tels algorithmes.

Abstract — ***A Review of Recent Advances in Discretization Methods*, a Posteriori *Error Analysis, and Adaptive Algorithms for Numerical Modeling in Geosciences*** — *Two research subjects in geosciences which lately underwent significant progress are treated in this review. In the first part, we focus on one key ingredient for the numerical approximation of the Darcy flow problem, namely the discretization of diffusion terms on general polygonal/polyhedral meshes. We present different schemes and discuss in detail their fundamental numerical properties such as stability, consistency, and robustness. The second part of the paper is devoted to error control and adaptivity for model problems in geosciences. We present the available* a posteriori *estimates guaranteeing the maximal overall error and show how the different error components can be identified. These estimates are used to formulate adaptive stopping criteria for linear and nonlinear solvers, time step choice adjustment, and adaptive mesh refinement. Numerical experiments illustrate such entirely adaptive algorithms.*

INTRODUCTION

Recently, there has been an increased interest and significant progress in two subjects related to the numerical approximation of problems in geosciences: the conception of novel discretization schemes for diffusion terms on almost arbitrary polygonal/polyhedral meshes, and the development of *a posteriori* error estimates and of adaptive algorithms. The study of new schemes is a key ingredient to simulate more realistic models including complex geometric features and physical properties. The use of *a posteriori*-driven algorithms is a promising way of compensating the increased computational cost for complex models. This paper provides an overview of some recent advances in both fields. The material is organized as follows.

In Section 1, we introduce the basic model of geosciences treated in this work, the compositional multiphase Darcy flow problem. Its sub-models, the single-phase steady, single-phase unsteady, and two-phase immiscible incompressible unsteady Darcy flow problems will also be considered in the paper in order to pertinently illustrate individual issues.

Section 2 summarizes some recent advances in discretization schemes for diffusion terms on general polygonal/polyhedral meshes. After discussing some general properties that are relevant both from the theoretical and practical point of view, we briefly present three families of numerical methods which have received extensive attention over the last few years. More specifically, Section 2.3 is devoted to multi-point finite volume (and mixed finite element) methods, Section 2.4 presents a few examples of lowest-order variational methods, and Section 2.5 focuses on discontinuous Galerkin methods. For all the methods, we provide a concise introduction stating the main principles, some examples of actual schemes, and discuss their properties in detail. In the discussion, we pay special attention to practical issues concerning the implementation and/or the integration into existing codes.

In Section 3, we then present fully computable, guaranteed *a posteriori* error estimates successively for the three sub-models mentioned above and for the compositional model itself. These estimates allow us to certify the error committed in a numerical approximation. Moreover, they enable to distinguish and estimate separately the different error components, such as the spatial discretization error, the temporal discretization error, the linearization error, or the algebraic solver error. This distinction then gives rise to entirely adaptive algorithms, where, in addition to the common time step choice and adaptive mesh refinement, the linear and nonlinear iterative solvers are steered by adaptive stopping criteria. We shall see that this typically leads to important computational savings.

1 THE COMPOSITIONAL DARCY MODEL

The compositional Darcy model describes the flow of several fluids through a porous medium occupying the space region $\Omega \subset \mathbb{R}^d$, $d = 2, 3$, over the time interval $(0, t_F)$. We consider a system where matter is present in different liquid or gas *phases* from the set $\mathcal{P} = \{p\}$, each containing one or more *components* from the set $\mathcal{C} = \{c\}$. The number of phases and components are respectively denoted by $N_\mathcal{P}$ and $N_\mathcal{C}$. A synthetic description of the system which accounts for the fact that a component may only be present in selected phases is provided by the binary component-phase matrix $\mathbf{M} = (m_{cp})_{c\in\mathcal{C},\, p\in\mathcal{P}}$ such that, for all $c \in \mathcal{C}$ and all $p \in \mathcal{P}$:

$$m_{cp} = \begin{cases} 1 & \text{if the component } c \text{ is present in the phase } p \\ 0 & \text{otherwise} \end{cases}$$

For all $c \in \mathcal{C}$, we denote by $\mathcal{P}_c \subset \mathcal{P}$ the set of phases in which the component c is present. Symmetrically, for all $p \in \mathcal{P}$, $\mathcal{C}_p \subset \mathcal{C}$ denotes the set of components present in the phase p. The governing equations are inferred from the general principles of mass and energy conservation supplemented by a suitable set of algebraic closure relations. For the sake of simplicity, it is assumed in what follows that all the phases are present. When this is not the case, the model can be modified as outlined in the work of Coats *et al.* [1], where an additional, discrete-valued unknown accounting for the phases present in each point of the domain is added associated to a flash calculation to enforce local equilibrium. In what follows we also assume that the temperature is fixed and uniform and that no energy source or sink is present, so that the energy balance is trivially verified.

Following [1], the unknowns of the model are the reference pressure P, the saturations S_p defined as the volumetric fraction occupied by the phase $p \in \mathcal{P}$, and the molar fractions $C_{p,c}$ of each component $c \in \mathcal{C}$ in the phases $p \in \mathcal{P}_c$ in which it is present. It is convenient, for all $p \in \mathcal{P}$, to define the vector of molar fractions $\mathbf{C}_p := (C_{c,p})_{c\in\mathcal{C}_p}$. While other choices are possible for the set of unknowns, this one lends itself to discretizations with arbitrary levels of implicitness in the time integration schemes and milder nonlinearities according to [2]. For all $p \in \mathcal{P}$, the phase pressure P_p is obtained by adding the capillary pressure to the reference pressure:

$$P_p := P + P_{c_p}$$

The reference pressure P can be chosen equal to the pressure of a given phase. In this case, the corresponding capillary pressure is identically zero. A more general choice consists in using as a reference pressure a linear combination of the phase pressures.

The tensor-valued absolute permeability and the porosity of the medium are denoted by $\mathbf{K}$ and ϕ, respectively. For each phase $p \in \mathcal{P}$, the following properties are relevant to the model (the usual dependence on the unknowns of the model is provided in brackets):

- molar density, $\zeta_p(P_p, \mathbf{C}_p)$;
- mass density, $\rho_p(P_p, \mathbf{C}_p)$;
- viscosity, $\mu_p(P_p, \mathbf{C}_p)$;
- capillary pressure, $P_{c_p}(S_p)$;
- relative permeability, $k_{r_p}(S_p)$.

To account for the presence of injection or production wells, for all $c \in \mathcal{C}$ we denote by q_c a source field defined on the space-time domain $\Omega \times (0, t_F)$. A detailed treatment of well models is out of the scope of the present review, and is, in perspective, an interesting addition to both the topics addressed herein. For a discussion on the modeling of singularities in the context of reservoir engineering, we refer, *e.g.*, to Ding and Jeannin [3]. The mass balance for each component yields:

$$\partial_t n_c + \sum_{p \in \mathcal{P}_c} \nabla \cdot \left(\frac{\zeta_p k_{r_p}}{\mu_p} \mathrm{C}_{p,c} \boldsymbol{u}_p \right) = q_c \qquad \forall c \in \mathcal{C} \tag{1a}$$

where n_c denotes the number of moles for the component c and, for all $p \in \mathcal{P}$, the average phase velocity is given by Darcy's law ($\boldsymbol{g}$ denotes the upward-oriented gravity acceleration):

$$\boldsymbol{u}_p = -\mathbf{K}(\nabla P_p + \rho_p \boldsymbol{g}) \tag{1b}$$

The pore-volume conservation principle states that the sum of the saturations is equal to one in each point of the space-time domain, as expressed by the following algebraic equation:

$$\sum_{p \in \mathcal{P}} S_p = 1 \tag{1c}$$

The phase quantity of matter conservation principle requires that the sum of the molar fractions of the components present in a given phase be equal to one:

$$\sum_{c \in \mathcal{C}_p} C_{p,c} = 1 \quad \forall p \in \mathcal{P} \tag{1d}$$

Additional algebraic laws are obtained by enforcing the equality of component fugacities, which corresponds to assuming thermodynamic equilibrium in mass transfer between phases. For simplicity of exposition, this topic is not addressed here, and we refer to [1, 4] for further details. Finally, we assume that the system (1) is supplemented with no-flow boundary conditions and that suitable initial conditions are derived, by an equilibrium computation.

2 DISCRETIZATION OF DIFFUSIVE TERMS

2.1 General Considerations

One of the key ingredients of numerical methods for the compositional Darcy problem of Section 1 is the discretization of diffusive terms $-\mathbf{K}\nabla P_p$, $p \in \mathcal{P}$, appearing in the expression of the average phase velocity (1b). From the model standpoint, the permeability field $\mathbf{K}$ displays strong heterogeneities reflecting the different mineral composition of geological layers. In addition, the upscaling of fine scale heterogeneities or of extensive fracturing can result in full permeability tensors with large anisotropy ratios. From the discretization standpoint, mesh generation is often performed in a separate stage, and is focused on integrating physical and geometric data from the seismic analysis. As a result, fairly general meshes can be encountered, featuring, *e.g.*, nonmatching interfaces corresponding to geological faults or general polyhedral elements resulting from the degeneration of hexahedral cells in eroded layers. This is notably the case in basin modeling, where deposition and erosion as well as fracturing must be accounted for owing to the long time scales. In reservoir modeling, polyhedral elements may also be present in near wellbore regions, where the use of radial meshes can be prompted by (qualitative) *a priori* knowledge of the solution. Nonconforming h-refinement can also appear at specific locations where the resolution needs to be increased or when moving fronts are present [2].

Identifying an appropriate discretization of diffusive terms is not an easy task, since several and often mutually contradictory requirements come into play. The most relevant (in our opinion) can be summarized as follows.

2.1.1 Consistency on general polyhedral meshes and for heterogeneous and anisotropic tensors

Roughly speaking, consistency expresses the fact that the discrete problem is "not too distant" from the continuous one. There are several ways of formulating consistency, either by requiring that the continuous problem is recovered by extending the discrete formulation to the continuous one in the limit, or by demanding that

the discrete problem yields the exact solution in certain circumstances. The latter formulation is sometimes referred to as the patch test [5, Chapter 10]. It is well known that the classical Two-Point Finite Volume method (TPFV) is consistent only on superadmissible meshes for which the line segments joining the center of a cell and the barycenters of its faces are $\mathbf{K}^{-1}$-orthogonal to the corresponding face [6, Lemma 2.1].

2.1.2 Robustness with respect to the permeability tensor

Technically speaking, robustness is achieved if error estimates are available that are uniform with respect to $\mathbf{K}$ [7] for a discussion on the robustness of a diffusion-advection model in the presence of impermeable regions. In practice, this means that the discretization error can be bounded in terms of a product of a constant independent of $\mathbf{K}$ and a power of the meshsize. Of course, this is only possible if the method is appropriately designed and a suitable error measure is chosen.

2.1.3 Stability

Stability is the ability of the scheme to prevent the amplification of numerical errors. While the consistency requirement has been well assimilated by practitioners, this is often not the case for the equally important stability requirement. In what follows, we will mainly focus on stability in an energy-like or similar norm, which is a sufficient requirement for convergence in the linear case. Most of the modern schemes successfully embed this principle. In the nonlinear case, however, tighter forms of stability are required, which are not easy to obtain at the discrete level. A particularly relevant form for degenerate parabolic problems is the discrete maximum principle, which essentially states that, under suitable conditions, the extrema of the solution are to be found on the boundary of the domain. This topic is not addressed in detail in the following discussion. For further insight on the role of the maximum principle in proving the convergence of discretization schemes for the Darcy problem, the reader may consult [8, Chapter 6] and the references therein. A particularly instructive convergence study of a Finite Volume (FV) method on superadmissible meshes for unsteady advection-diffusion problems is carried out by Gallouët *et al.* [9]. A Discrete-Duality Finite Volume (DDFV) method for a large class of nonlinear degenerate hyperbolic-parabolic problems is considered [10] under assumptions on the mesh that allow us to infer a discrete maximum principle. Numerical enforcement of the maximum principle by nonlinear corrections is considered [11], to which we also refer for an up-to-date bibliographic section on this topic.

2.1.4 Low Computational Cost

Low computational cost, both in terms of CPU time and parallel communications, is a key requirement in industrial codes, since competition is often based on reducing the simulation time rather than on improving the resolution of the model. The demand for faster simulators is reflected in different ways in the design of numerical schemes. First, with the notable exception of the energy equation in basin modeling, it is generally admitted that lowest-order methods are the sole offering an acceptable trade-off between precision and simulation time. More generally, a great care must be spent to avoid the explosion of the number of unknowns while still meeting the previous requirements. Second, the stencil of the scheme should be as compact as possible in order to limit the amount of data exchange in parallel executions. Indeed, on the one hand, the trend for computer manufacturers is to increase computing power by adding multiple cores on a single processor rather than increasing the speed of each core; on the other hand, the users of commercial simulators are often interested in increasing the complexity of the model rather than the mesh resolution. As a result, achieving parallel efficiency requires to handle situations where heavy computations are performed on (relatively) few cells on each processor. In such circumstances, boundary cells and, hence, parallel data exchanges, have a major impact on the overall simulation time. Another related aspect is the availability of efficient parallel preconditioners for the linear systems arising from the discretization and the linearization of the Darcy problem. Although this topic is not addressed in detail here, it is usually acknowledged that (relatively) standard preconditioners such as the algebraic multigrid Boomer AMG available in the Hypre library [12] perform well when FV or FV-like methods are used and mild heterogeneities are present, while this is not always the case when discontinuous Galerkin (dG) discretizations are employed. The issue of devising good preconditioners for highly heterogeneous problems is an active field of research. For a discussion on this topic as well as for an up-to-date bibliographic section [13-15]. When it comes to dG methods, one of the very few contributions available is the work of Ayuso de Dios and Zikatanov [16].

2.1.5 Local conservation on the computational mesh

Local conservation is a somewhat controversial point, since it does not seem mandatory from the analysis point of view. Moreover, possibly after minor modifications or after a reconstruction postprocessing procedure, most discretization methods can exhibit conservation properties: [17] for mixed finite element and nonconforming finite element methods on general polygonal meshes, [18] for cell-centered Galerkin methods, [6, 19] for nonconforming finite element and generalized FV methods, [20-22] for dG methods and [23–27] for conforming finite element methods. For the purposes of the present work this property will hence be intended as the availability of a simple expression for the flux and the Darcy velocity (1b) rather than its sheer existence. Note that the possibility of reconstructing locally conservative Darcy fluxes is a key ingredient for the *a posteriori* analysis of Section 3, see Assumptions 2, 4, and 6 therein. It is thus in this point that a strong connection between the scheme conception and understanding and *a posteriori* analysis appears.

2.1.6 Integrability into Existing Simulators

This last point is essentially dictated by practical considerations. The lifespan of an industrial simulator is usually of ten years or more, and it is possibly only slightly shorter when it comes to large-scale academic codes. During this time, innovations are usually incremental and major changes to incorporate new schemes may only be considered if a clear trade-off can be identified. As a result, coping with existing codes can play a major role in deciding which numerical method is best-suited for the application at hand. The most widely used industrial reservoir simulators are based on traditional FV methods, and modifications to include radically different schemes are not necessarily possible or economically viable. Similar considerations also apply to large-scale academic simulators. The advances both in the understanding of discretization methods and in the flexibility of programming languages have prompted recent projects to build upon generic bricks that allow to easily modify the numerical formulation. In the context of geosciences, an example is provided by the recent work [28, 29] based on the proprietary platform Arcane [30] and inspired by similar tools for finite element methods [31], whereas an open source example is provided by the DuMuX project [32].

2.2 Model Problem and Notation

In the rest of this section, we briefly review some relevant advances in the development and analysis of numerical schemes for diffusive terms, and highlight the characteristics of each method based on the points listed in Section 2.1. For the sake of simplicity, our main focus is on the steady linear model problem:

$$\begin{aligned} -\nabla\cdot(\mathbf{K}\nabla u) &= f \quad \text{in } \Omega \\ u &= 0 \quad \text{on } \partial\Omega \end{aligned} \tag{2}$$

where Ω denotes the spatial domain and f models a source term. Problem (2) coincides with the single-phase, single-component ($N_P = N_C = 1$) Darcy problem provided gravitational effects are neglected. In this case, u represents the (unique) phase pressure. The interest in problem (2) is not merely theoretical, as it is used in practice as a starting point to infer an expression for the diffusive term $-\mathbf{K}\nabla P_p$, $p \in \mathcal{P}$, in the compositional model of Section 1.

In what follows we denote by $\mathcal{T}_h = \{T\}$ a mesh, that is to say, a collection of open polyhedra called cells or elements such that $\Sigma_{T\in\mathcal{T}_h}\bar{T} = \bar{\Omega}$. The notion of general mesh is related to the range of element shapes and arrangements for which the numerical scheme possesses the mathematical requirements of consistency and stability. As such, its precise definition depends on the scheme itself. Moreover, it is often not possible to provide an optimal definition of admissible mesh, but only formulate sufficient conditions based on computable quantities. In practice, we would like to be able to treat (at least) all meaningful degenerate elements obtained by suppressing edges of a quadrilaterally-faced hexahedron. Such elements are encountered in basin modeling as a result of erosion. In reservoir modeling, we may also be interested in allowing more general polyhedral elements to discretize the near wellbore region. A mesh $\mathcal{T}_h$ is primarily caracterized by a linear dimension h corresponding to the largest diameter of its elements. We say that a method is convergent if a suitable measure of the error tends to zero when h does so. From a mathematical viewpoint, convergence is equivalent to stability for a consistent method (this result is sometimes referred to as the Lax-Ritchmyer theorem).

An important notion for all the discretization methods discussed in what follows is that of interface, which defines the way two elements can come into contact. Here, a basic requirement is that nonmatching interfaces should be supported, *i.e.*, two neighboring elements should be allowed to share only portions of their faces. In basin modeling, nonmatching interfaces may be used to represent faults; in reservoir modeling they may appear as a consequence of nonconforming h-adaptivity, *i.e.*, the increase of the local mesh resolution obtained by subdiving a mesh element leaving its neighbors untouched. The definition of interface may

vary from one method to another. As an example, interfaces are connected and planar for the SUSHI method of [6], while they can be defined as the intersection of two elements (hence non necessarily planar and possibly non connected) when it comes to dG methods [22, 33] for a discussion on this subject. For the multi-point finite volume and lowest-order methods treated in Sections 2.3 and 2.4 respectively, the planarity requirement on faces may seem stringent in three space dimensions. However, nonplanar faces can usually be efficiently treated by approximating them by a split into planar subfaces. For a rigorous treatment of non planar faces in the context of Mimetic Finite Difference Methods (MFDM) [48]. In what follows, the set of interfaces is denoted by $\mathcal{F}_h^{\mathrm{i}}$, the set of boundary faces by $\mathcal{F}_h^{\mathrm{b}}$ and we let $\mathcal{F}_h := \mathcal{F}_h^{\mathrm{i}} \cup \mathcal{F}_h^{\mathrm{b}}$. For every element $T \in \mathcal{T}_h$, we denote by $\mathcal{F}_T$ the set of faces that lie on the boundary of T. For every interface $F \in \mathcal{F}_h^{\mathrm{i}}$, we choose an arbitrary but fixed orientation for the unit normal $\boldsymbol{n}_F$ and enumerate the elements $T_1, T_2 \in \mathcal{T}_h$ such that $F \subset \partial T_1 \cap \partial T_2$ so that the outward unit normal $\boldsymbol{n}_{T_1,F}$ coincides with $\boldsymbol{n}_F$.

Henceforth, we assume that $\mathbf{K}$ is piecewise constant on the mesh $\mathcal{T}_h$, *i.e.*, jumps in the permeability can only occur at interfaces. In practice, this assumption is always verified in geological modeling since the computational mesh is used as a support for the physical properties.

2.3 Multi-Point Finite Volume Methods

2.3.1 Principles

A class of schemes that is nowadays very popular in the oil industry is that of Multi-Point Finite Volume methods (MPFV), independently introduced in the 90s [34, 35]. The key idea of MPFV methods is to recover consistency on general meshes by extending the dependence of diffusive fluxes to cell unknowns other than the ones associated to the cells sharing a face. The coefficient associated to each cell unknown is usually obtained by solving a local problem. In what follows we exemplify these ideas by outlining the G-method [36], which generalizes the L-method [37]. For a survey of other constructions, we refer to Aavatsmark [38]. We cite, in particular, the O-method, for which a convergence analysis under very general assumptions on the permeability tensor has been recently [39].

The FV discretization of problem (2) reads:

$$-\sum_{F\in\mathcal{F}_T} |F|_{d-1}\Phi_{T,F} = \langle f\rangle_T |T|_d \quad \forall T \in \mathcal{T}_h \tag{3}$$

where $\langle f\rangle_T := |T|_d^{-1}\int_T f$ and $(\Phi_{T,F})_{T\in\mathcal{T}_h, F\in\mathcal{F}_T}$ are *numerical fluxes* which satisfy the following local conservation property:

$$\forall F \in \mathcal{F}_h^{\mathrm{i}},\ F \subset \partial T_1 \cap \partial T_2,\ \Phi_F := \Phi_{T_1,F} = -\Phi_{T_2,F} \tag{4}$$

The single-valued quantity Φ_F is termed *interface flux*. In the TPFV method, the interface flux only depends on the (scalar-valued) cell unknowns u_{T_1} and u_{T_2} which are meant to approximate representative values of the solution in the cells T_1 and T_2, respectively. More specifically, for all $T \in \mathcal{T}_h$, we identify a point $\boldsymbol{x}_T \in T$ away from the boundary of T to which the value u_T is associated. For all $T \in \mathcal{T}_h$ and all $F \in \mathcal{F}_T$, denote by $d_{T,F}$ the orthogonal distance between $\mathbf{x}_T$ and F. Using a finite difference approximation of the directional derivative along $\boldsymbol{n}_F$ and enforcing relation (4), we infer:

$$\Phi_F = \frac{\alpha_1\alpha_2}{\alpha_1+\alpha_2}(u_{T_2}-u_{T_1}),\ \alpha_i := \frac{\mathbf{K}_{|T_i}\boldsymbol{n}_F\cdot\boldsymbol{n}_F}{d_{T_i,F}}$$

This expression yields a consistent method only if the mesh satisfies the superadmissibility condition [6, Lemma 2.1]. To remedy this lack of consistency, Aavatsmark *et al.* [37] propose a local reconstruction based on $d+1$ cells which share a same node usually referred to as the L-method. In Figure 1a, we show a two-dimensional example where these faces are denoted by F_1 and F_2. The key idea is to reconstruct a piecewise affine function on the gray patch only depending on the values of the unknowns u_T, u_{T_1}, and u_{T_2} and of the permeability field in the cells T, T_1, and T_2. This piecewise affine reconstruction is obtained by enforcing pressure continuity and flux conservation across F_1 and F_2. The interface fluxes Φ_{F_1} and Φ_{F_2} are then obtained replacing the exact solution u by the piecewise affine reconstruction in the expression $-(\mathbf{K}\nabla u)_{|T}\cdot\boldsymbol{n}_{F_i}$, $i\in\{1,2\}$. It can be shown that this reconstruction requires the solution of a $d\times d$ linear system. An explicit expression for the entries of the system is provided in [36, Lemma 3.1], to which we refer for a more formal and detailed presentation. When the permeability field is heterogeneous, this construction outperforms a Lagrange interpolation based on the cell values u_T, u_{T_1}, u_{T_2} in terms of consistency, since the resulting piecewise gradient embeds a dependence on the jumps of $\mathbf{K}$ *via* Equation (4).

It is a simple matter to realize that, for a given interface $F \in \mathcal{F}_h^{\mathrm{i}}$, there are multiple choices for a second face to perform the construction outlined above (*Fig. 1b*). As a result, several different flux expressions are in principle available. The key idea of the G-method is to define Φ_F as a linear combination of all possible fluxes with weights chosen in such a way as to enhance a selected

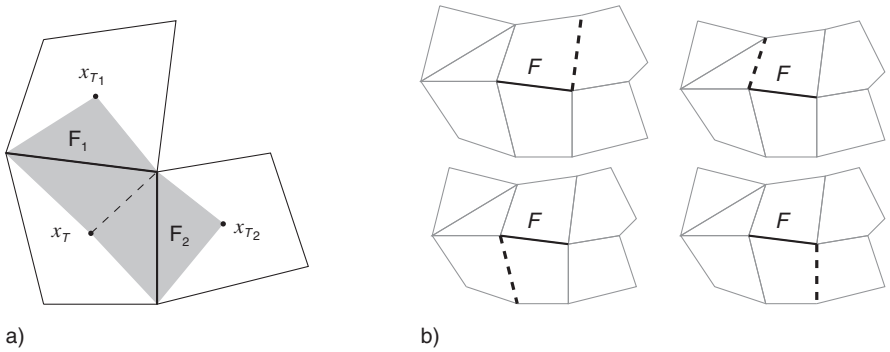

Figure 1

Local reconstruction. a) Notation; b) possible choices for the second face used to reconstruct Φ_F (thick dashed lines).

property for the method. A criterion geared towards increased stability is proposed in [36, Section 3.4]. In a different context where the construction is used as a trace interpolator, an accuracy-oriented criterion is discussed in [40, Section 2.3].

2.3.2 A Numerical Example in Basin Modeling

To assess the properties of the G-method method and provide a comparison with the other methods discussed in what follows, we consider the benchmark problem in basin modeling originally proposed in [36]. The results are obtained using the unified implementation discussed in [29]. Convergence is studied on a mesh family obtained by successive refinements of the two-dimensional basin mesh depicted in Figure 2, which contains both quadrangular and triangular elements as a result of erosion. We consider the following analytical solution:

$$u(\boldsymbol{x}) = \sin(\pi x_1)\sin(\pi x_2), \quad \mathbf{K} = \begin{bmatrix} \epsilon & 0 \\ 0 & 1 \end{bmatrix} \tag{5}$$

with the right-hand side f determined by (2). The anisotropy ratio ϵ is taken equal to 0.1, corresponding to a permeability which is ten times smaller in the vertical than in the horizontal direction.

In Figure 3, we evaluate the performance of several schemes including the G-method, with respect to different metrics. Accuracy is evaluated in terms of the error on the pressure (L^2-error) and on its gradient (H^1-error), both computed with a quadrature rule using the cell center as a quadrature node. For multi-point schemes, a piecewise constant gradient was reconstructed according to [36, Equation (2.5)]. We emphasize that the error on the gradient is perhaps the most significant measure, since it closely relates to fluxes, which are the quantities of interest in oil-related problems. The order of convergence is classically expressed relating the error to the meshsize h, and it measures how fast the error tends to zero as the meshsize does so. When dealing with solutions that are sufficiently regular, one can expect that the error scales as a power of h, corresponding to the different slopes of the curves in the log-log plots of Figures 3a and 3b. Since the comparison includes schemes which feature a different number of unknowns for a given

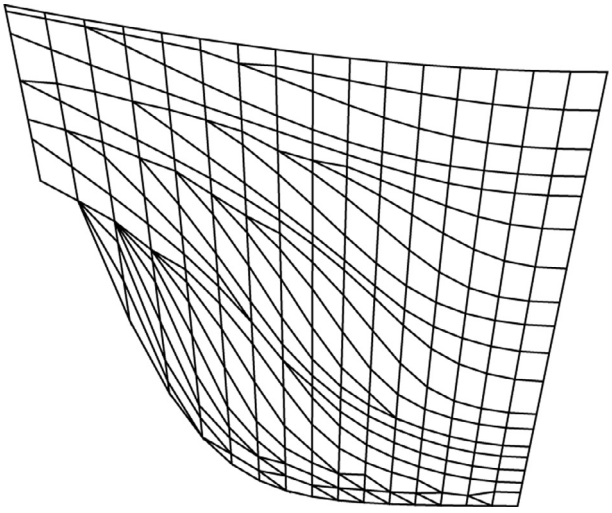

Figure 2

Two-dimensional stratigraphic mesh. The actual aspect ratio is $x{:}y = 10{:}1$.

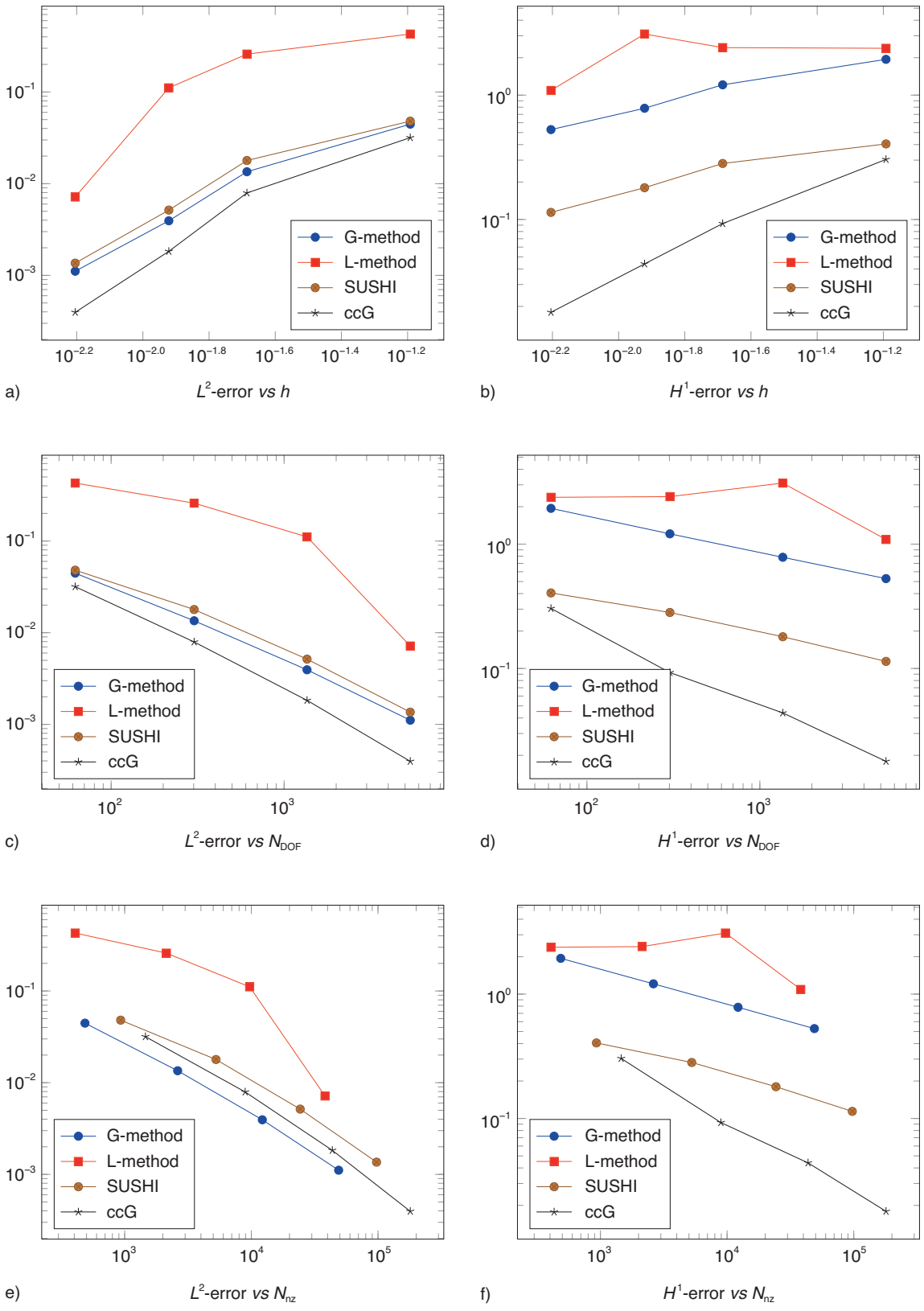

Figure 3

Accuracy and memory consumption analysis for example (2) in basin modeling. The ccG scheme is detailed in Section 2.4.2. The data are taken from reference [29].

mesh, a fairer comparison consists in relating the error to the number of unknowns N_{DOF}, which we do in Figures 3c and 3d. The memory consumption can be evaluated by plotting the error as a function of the number of nonzero entries in the linear system corresponding to the discretization of problem (2), which is the contents of Figures 3e and 3f.

2.3.3 Discussion

We conclude by summarizing the features of MPFV methods in terms of the points identified in Section 2.1:

- consistency. The comparison in Figures 3a-d shows that, although MPFV are consistent by construction, the lack of an embedded stability mechanism sometimes results in the loss of convergence. This is the case, *e.g.*, for the L-method on the first three levels of mesh refinement. Moreover, while MPFV methods stand the competition when the L^2-error is considered, this is often not the case for the H^1-error;
- robustness. The local problems introduced to construct numerical fluxes in MPFV methods embed a dependence on the permeability tensor. In a way, this adds to the robustness of the method since accuracy may be retained in the heterogeneous anisotropic case. In some cases, however, the conditioning of the local problems may be dramatically affected by rough permeability tensors, resulting in highly inaccurate reconstructions. For some methods, the local problems may even be ill-posed, and backup strategies must be devised; for the G-method [36, Section 3.1]; for the O-method [41, Example 3.10], and [17, Remark 4.2];
- stability. As we have already mentioned, convergence may sometimes be lost owing to the absence of an intrinsic stability mechanism in MPFV methods. Although stability can be proved in some circumstances [36, Lemma 3.4], this typically requires assumptions on the mesh *and* on the permeability tensor that are either too stringent or difficult to check in practice;
- low computational cost. This is one of the key advantages of MPFV methods, which feature only one unknown per cell as is the case for the classical TPFV method. A major difference is, however, that the stencil is typically extended to the neighbors in the sense of nodes. While this is acceptable in most of the cases (most notably for quasi-hexahedral meshes), it can sometimes lead to very large stencils when tetrahedral meshes are used. The difference with respect to other methods can be appreciated, *e.g.*, in Figures 3e and 3f. As regards the solution of the resulting linear system, one point that deserves to be mentioned is that AMG preconditioners may be less efficient than in the TPFV case since the global matrix is no longer an M-matrix. When stability is lost, the presence of eigenvalues with opposite sign may significantly affect the solution of the linear system (even when the solution remains unique);
- local conservation. MPFV are classical finite volume methods, hence they inherently provide a simple expression for interface fluxes;
- integrability into existing simulators. A common practice in finite volume codes is to express the links between cells in terms of a graph. MPFV methods naturally fit this approach, since the sole difference with respect to the TPFV scheme lies in the number of connections. In this respect, they are the easiest method to integrate into existing simulators. A possible difficulty that deserves to be mentioned is that the stencil of MPFV methods includes neighbors in the sense of nodes, which may require to redesign the communication patterns in parallel codes.

2.3.4 Mixed Finite Element Methods

We would like to emphasize here that mixed finite element methods, in particular the lowest-order Raviart-Thomas scheme, [42, 43], can be viewed as a member of the MPFV family. Indeed [44, 41], they can likewise be implemented with one unknown per mesh element and local flux expressions can be obtained upon solution of local problems on patches of elements. They are in particular tightly related to the MPFA O-method on simplicial meshes (with the matrix equivalent in two space dimensions) [41, 45, 46]. Moreover, mixed finite elements can easily be defined on general polygonal/polyhedral meshes [17]. At the same time, they do not suffer from the loss of convergence as discussed in point "Consistency" in Section 2.3.3 above and as observed in Figure 3, neither they exhibit stability problems as those discussed in point "Stability" in Section 2.3.3 above. A detailed discussion of these issues can be found in [17].

2.4 Variational Lowest-Order Methods on General Meshes

2.4.1 Principles

In recent years, several new methods have been proposed that successfully address the stability issues of MPFV methods. These methods include, in particular, the Mimetic Finite Difference (MFD) methods of Brezzi *et al.* [47-49], the Hybrid Finite Volume (HFV) methods of Eymard *et al.* [6, 50], the Mixed Finite Volume (MFV) method of Droniou and Eymard [51], the finite volume vision of mixed finite elements [17, 41], and the

cell-centered Galerkin methods introduced in [40, 52]. The close relation between these methods has been recently investigated in [53, 54], where a different formalism is presented leading to Gradient Schemes; [17] gives yet another equivalence viewpoint. Another emerging formalism that deserves to be mentioned is that of Compatible Discrete Operators (CDO) recently proposed by Bonelle and Ern [55]. We would also like to mention at this point the recent review by Droniou [56], which contains several complements with respect to the present work. In what follows we collectively refer to these methods as Variational Lowest-Order (VLO) methods. While this naming is by no means standard, it underlines the fact that, unlike classical finite volume methods, they are inspired by the weak formulation of the problem.

These schemes rely on a weak or variational formulation and often share significant similarities with mixed or nonconforming Finite Element (FE) methods. To illustrate some important ideas, we focus on two examples that are related to nonconforming FE methods. In what follows we assume for the sake of simplicity that the source term f is square-integrable. Moreover, zero pressure boundary conditions are considered, so that the natural space for the solution is $V := H_0^1(\Omega)$ (the space of square-integrable functions with square-integrable weak derivatives that vanish on $\partial\Omega$). The weak formulation of problem (2) consists in finding $u \in V$ such that:

$$a(u,v) := \int_\Omega \mathbf{K}\nabla u \cdot \nabla v = \int_\Omega fv \quad \forall v \in V \tag{6}$$

Problem (6) classically admits a unique solution as a consequence of the Poincaré inequality:

$$||v||_{L^2(\Omega)} \leq C_\Omega ||\nabla v||_{L^2(\Omega)^d} \tag{7}$$

where $C_\Omega > 0$ only depends on the spatial domain Ω. Inequality (7) states that the L^2-norm of the gradient is a norm and not just a seminorm in V. In other words, if a function $v \in V$ is such that $||\nabla v||_{L^2(\Omega)^d} = 0$, then v is the null function. This allows, in particular, to infer a stability result for the bilinear form a provided the permeability tensor $\mathbf{K}$ is uniformly elliptic. This means that diffusion occurs along every direction at every point of a cell.

To formulate a convergent approximate version of (6), it is necessary to devise a bilinear form a_h which:

- provides a good approximation of a, *i.e.*, is consistent possibly up to an error which decreases with the mesh-size h;
- is stable based on a discrete version of (7). A key ingredient for obtaining these properties is to design a suitable approximation of the gradient.

2.4.2 Hybrid Finite Volume and Cell-Centered Galerkin Methods

In this section, we present two examples of VLO methods which, up to minor modifications, were proposed in [6, 40], respectively.

A remark that can be exploited to design a gradient approximation is that Green's formula [57, Theorem 3.2.1] together with the planarity of faces yields, for all $T \in \mathcal{T}_h$ and v smooth enough:

$$|T|_d \langle \nabla v \rangle_T = \int_T \nabla v = \int_{\partial T} v \boldsymbol{n}_T = \sum_{F \in \mathcal{F}_T} |F|_{d-1} \langle v \rangle_F \boldsymbol{n}_{T,F} \tag{8}$$

where, for $X \subset \overline{\Omega}$, $\langle \varphi \rangle_X$ denotes the average value of φ on X, while $\boldsymbol{n}_{T,F}$ is the unit normal to F pointing out of T. Equation (8) suggests that, introducing the face unknowns $\mathbb{v}_\mathcal{F} := (v_F)_{F \in \mathcal{F}_h}$ and interpreting them as average values over faces, a gradient approximation is given by the piecewise constant function $\boldsymbol{G}_h(\mathbb{v}_\mathcal{F})$ such that:

$$\boldsymbol{G}_h(\mathbb{v}_\mathcal{F})_{|T} = \boldsymbol{G}_T(\mathbb{v}_\mathcal{F}) \equiv \frac{1}{|T|_d} \sum_{F \in \mathcal{F}_T} |F|_{d-1} v_F \boldsymbol{n}_{T,F} \quad \forall T \in \mathcal{T}_h \tag{9}$$

This choice is consistent in the following sense. For all $v \in V$, letting $\mathbb{v}_\mathcal{F} = (\langle v \rangle_F)_{F \in \mathcal{F}_h}$, there holds:

$$\boldsymbol{G}_h(\mathbb{v}_\mathcal{F})_{|T} = \langle \nabla v \rangle_T \quad \forall T \in \mathcal{T}_h \tag{10}$$

It is assumed henceforth that $v_F = 0$ for all $F \in \mathcal{F}_h^b$, which amounts to strongly enforcing the zero pressure boundary condition. A drawback of the gradient approximation defined by (9) is that it does not satisfy a discrete version of (7), that is to say, one can have $||\boldsymbol{G}_h(\mathbb{v}_\mathcal{F})||_{L^2(\Omega)^d} = 0$ even if $\mathbb{v}_\mathcal{F}$ is not null. This is the case, *e.g.*, for the mesh depicted in Figure 4, where a (tedious) hand calculation shows that the matrix of the linear system obtained enforcing $\boldsymbol{G}_h(\mathbb{v}_\mathcal{F})_{|T} = 0$ for all $T \in \mathcal{T}_h$ has a kernel of dimension equal to 2.

Stabilizing Using Residuals

A possible strategy to recover a discrete Poincaré inequality consists in adding a consistent subgrid correction to the expression (9). For every cell $T \in \mathcal{T}_h$, we fix one interior point $\boldsymbol{x}_T \in T$ such that T is star-shaped with respect to $\boldsymbol{x}_T$. We introduce the cell unknowns $\mathbb{v}_\mathcal{T} := (v_T)_{T \in \mathcal{T}_h}$ which can be interpreted as approximations of the solution values at cell centers, and define the function $\mathcal{G}_h(\mathbb{v}_\mathcal{T}, \mathbb{v}_\mathcal{F})$ such that, for all $T \in \mathcal{T}_h$ and all $F \in \mathcal{F}_T$:

$$\mathcal{G}_h(\mathbb{v}_\mathcal{T}, \mathbb{v}_\mathcal{F})_{|\mathcal{P}_{T,F}} = \boldsymbol{G}_T(\mathbb{v}_\mathcal{F}) + \boldsymbol{R}_{T,F}(\mathbb{v}_\mathcal{T}, \mathbb{v}_\mathcal{F}) \tag{11}$$

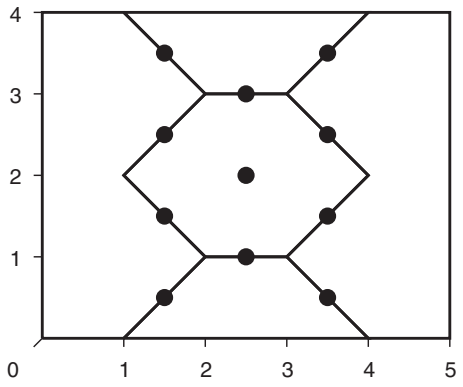

Figure 4

Example of polygonal mesh where the gradient reconstruction (9) does not satisfy a discrete Poincaré inequality. Interface unknowns are marked with a dot, boundary face unknowns are set equal to zero to strongly enforce the homogeneous Dirichlet boundary condition.

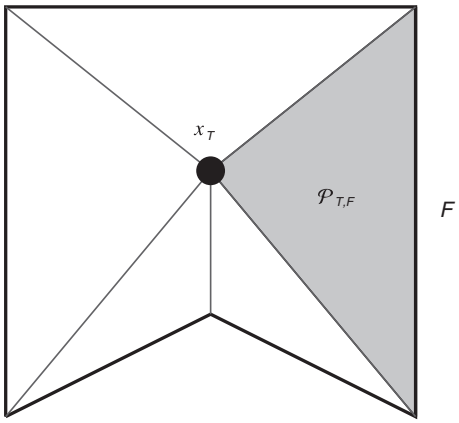

Figure 5

Cell center and face-based pyramid $\mathcal{P}_{T,F}$.

with $\mathcal{P}_{T,F}$ denoting the F-based pyramid with apex $\boldsymbol{x}_T$ (*Fig. 5*) and:

$$\boldsymbol{R}_{T,F}(\mathbb{v}_T,\mathbb{v}_{\mathcal{F}}) \equiv \frac{\eta}{d_{T,F}}(v_F - v_T - \boldsymbol{G}_T(\mathbb{v}_{\mathcal{F}})\cdot(\boldsymbol{x}_F-\boldsymbol{x}_T))\boldsymbol{n}_{T,F} \tag{12}$$

where $d_{T,F}$ denotes again the orthogonal distance between $\boldsymbol{x}_T$ and F, $\boldsymbol{x}_F$ is the barycenter of F, and $\eta > 0$ is a user-defined parameter. The discretization of (6) reads:
Find $\mathbb{u} := (\mathbb{u}_{\mathcal{T}}, \mathbb{u}_{\mathcal{F}})$ such that, for all $\mathbb{v} := (\mathbb{v}_{\mathcal{T}}, \mathbb{v}_{\mathcal{F}})$ there holds:

$$a_h^{\mathrm{hfv}}(\mathbb{u},\mathbb{v}) := \int_\Omega \mathbf{K}\boldsymbol{\mathcal{G}}_h(\mathbb{u})\cdot\boldsymbol{\mathcal{G}}_h(\mathbb{v}) = \sum_{T\in\mathcal{T}_h}|T|_d\langle f\rangle_T v_T \tag{13}$$

It can be shown that the bilinear form a_h^{hfv} admits the following alternative expression:

$$\begin{aligned} a_h^{\mathrm{hfv}}(\mathbb{u},\mathbb{v}) = &\sum_{T\in\mathcal{T}_h}|T|_d\mathbf{K}_{|T}\boldsymbol{G}_T(\mathbb{u}_{\mathcal{F}})\cdot\boldsymbol{G}_T(\mathbb{v}_{\mathcal{F}}) \\ &+\sum_{T\in\mathcal{T}_h}\sum_{F\in\mathcal{F}_T}|\mathcal{P}_{T,F}|_d\mathbf{K}_{|T}\boldsymbol{R}_{T,F}(\mathbb{u})\cdot\boldsymbol{R}_{T,F}(\mathbb{v}) \end{aligned} \tag{14}$$

To interpret the correction (12), we introduce the piecewise affine reconstruction $\mathfrak{R}_h$ such that, for all $T \in \mathcal{T}_h$

$$\mathfrak{R}_h(\mathbb{v})_{|T}(\boldsymbol{x}) = v_T + \boldsymbol{G}_T(\mathbb{v}_{\mathcal{F}})\cdot(\boldsymbol{x}-\boldsymbol{x}_T) \quad \forall \boldsymbol{x}\in T \tag{15}$$

where $\mathbb{v} := (\mathbb{v}_{\mathcal{T}}, \mathbb{v}_{\mathcal{F}})$. Plugging (15) into (12) yields:

$$\boldsymbol{R}_{T,F}(\mathbb{v}) = \frac{\eta}{d_{T,F}}(v_F - \langle\mathfrak{R}_h(\mathbb{v})\rangle_F)$$

As a result, since $|\mathcal{P}_{T,F}|_d = \frac{|F|_{d-1}d_{T,F}}{d}$, the term in the second line of (14) can be alternatively written:

$$\sum_{T\in\mathcal{T}_h}\sum_{F\in\mathcal{F}_T}\frac{\eta^2|F|_{d-1}}{d\,d_{T,F}}(u_F - \langle\mathfrak{R}_h(\mathbb{u})\rangle_F)(v_F - \langle\mathfrak{R}_h(\mathbb{v})\rangle_F)$$

which shows that it is nothing but a least squares penalization of the difference between u_F and $\langle\mathfrak{R}_h(\mathbb{u})\rangle_F$. The consistency of this term stems from the fact that it vanishes when the exact solution is piecewise affine on $\mathcal{T}_h$.

Different choices are possible for the penalty parameter η in (12). The choice $\eta = \sqrt{d}$ is advocated in [6] since it allows to recover the TPFV method on superadmissible meshes, whereas it has been recently shown in [19] that the choice $\eta = d$ leads to interesting analogies with the Crouzeix-Raviart element. The fact that the discrete gradient (11) satisfies a discrete Poincaré inequality has been proved in [6, Section 5.1] with finite volume techniques. An analogous result can be obtained with finite element techniques using [19, Proposition 15] together with [58, Theorem 6.1].

Stabilizing Using Jumps

Starting from (15), an alternative way of recovering a discrete Poincaré inequality is to introduce a least-square penalization of interface jumps inspired by the work of Arnold [59] leading to cell-centered Galerkin (ccG) methods. For all $F \in \mathcal{F}_h^{\mathrm{i}}$ with $F \subset \partial T_1 \cap \partial T_2$, we introduce the jump and (weighted) average operators defined by:

$$[\![\varphi]\!] := \varphi_{|T_1} - \varphi_{|T_2},\ \{\varphi\} := \frac{\lambda_2}{\lambda_1+\lambda_2}\varphi_{|T_1} + \frac{\lambda_1}{\lambda_1+\lambda_2}\varphi_{|T_2}$$

where $\lambda_i := \mathrm{K}_{|T_i}\boldsymbol{n}_F.\boldsymbol{n}_F$ represents the permeability in the normal direction. For the sake of brevity, on boundary faces we conventionally set $[\![\varphi]\!] = \{\varphi\} = \varphi$. Stability hinges in this case on the following discrete Poincaré inequality valid for piecewise H^1 functions on $\mathcal{T}_h$ (cf. [60] and also [22, Corollary 5.4]):

$$||v||_{L^2(\Omega)} \leq \sigma_2 \left(||\nabla_h v||^2_{L^2(\Omega)^d} + \sum_{F\in\mathcal{F}_h} h_F^{-1} ||[\![v]\!]||^2_{L^2(F)} \right)^{\frac{1}{2}}$$

where ∇_h denotes the element-by-element broken gradient operator and h_F is the face diameter. The penalization of jumps is realized by the bilinear form:

$$j_h(u,v) = \sum_{F\in\mathcal{F}_h} \int_F \eta \lambda_{\mathrm{har}} h_F^{-1} [\![u]\!][\![v]\!] \tag{16}$$

where $\lambda_{\mathrm{har}} = \lambda_1\lambda_2/(\lambda_1+\lambda_2)$ on interfaces and $\lambda_{\mathrm{har}} = \lambda$ on boundary faces, while $\eta > 0$ is a user-dependent parameter. Let $\mathbf{V}_h$ denote the vector space of cell- and face-DOFs, and let $V_h^{\mathrm{ccg}} := \mathfrak{R}_h(\mathbf{V}_h)$ be the space of piecewise affine functions obtained from the reconstruction (15). The discretization of problem (2) reads: Find $u_h \in V_h^{\mathrm{ccg}}$ such that:

$$a_h^{\mathrm{swip}}(u_h, v_h) = \int_\Omega f v_h \quad \forall v_h \in V_h^{\mathrm{ccg}} \tag{17}$$

where:

$$\begin{aligned} a_h^{\mathrm{swip}}(u_h, v_h) := & \int_\Omega \mathbf{K}\nabla_h u_h \cdot \nabla_h v_h + j_h(u_h, v_h) \\ & - \sum_{F\in\mathcal{F}_h} \int_F \Big\{ [\![u_h]\!] \{\mathbf{K}\nabla_h v_h\} \cdot \boldsymbol{n}_F \\ & + \{\mathbf{K}\nabla_h u_h\} \cdot \boldsymbol{n}_F [\![v_h]\!] \Big\} \end{aligned} \tag{18}$$

The terms in the first line of (18) are responsible for consistency and stability, whereas those in the second and third lines respectively ensure consistency and symmetry. The bilinear form (18) was introduced in the context of domain decomposition methods for degenerate advection-diffusion problems [61]. A general analysis for dG methods for degenerate advection-diffusion problems inspired by similar mechanisms was later established in [7]. We emphasize that in problem (17) we use the discrete space V_h^{ccg} instead of a full broken polynomial space (as is the case for dG methods). This results in fewer degrees of freedom with respect to the corresponding lowest-order dG method discussed in Section 2.5.

2.4.3 Discussion

It is useful to summarize the features of VLO methods with respect to the points identified in Section 2.1:

- consistency. Variational lowest-order methods are consistent on quite general meshes and often for heterogeneous anisotropic permeability tensors. In the examples of Section 2.4.2, this comes at the cost of introducing additional face unknowns in the construction. A possible remedy consists in eliminating face unknowns by interpolating their values in terms of cell-centered unknowns. In this case, special procedures are required to retain consistency when heterogeneities are present. For a discussion, we refer to [40, Section 2.3], where interpolation relies on the construction of [36];
- robustness. Unlike MPFV methods, VLO methods do not inherently require local constructions which may lead to ill-posed problems. On the other hand, the underlying discrete space has some degree of global regularity (*e.g.*, the continuity of face-averaged values proved in [19]), which narrows the range of singularities in the exact solution that can be accurately represented with respect to dG methods (cf. Section 2.5.1). Robustness with respect to $\mathbf{K}$ can be proved in some circumstances. The use of local interpolation procedures to reduce the number of unknowns, however, makes it difficult to obtain general results;
- stability. As discussed in Section 2.4.2, stability is ensured by introducing penalty terms that allow to control the L^2-norm of discrete functions in terms of the L^2-norm of the (reconstructed) gradient. However, tighter forms of stability such as the discrete maximum principle are generally not available;
- low computational cost. While the methods presented in Section 2.4.2 have more unknowns than cell-centered finite volume methods, several reduction strategies are available. As already mentioned, one possibility consists in interpolating face unknowns in terms of cell unknowns. Although the local constructions required for interpolation have similar problems as the ones used in MPFV methods, this can be fixed by locally maintaining face unknowns as proposed in [6]. In general, the stencils of the resulting methods are larger than those of MPFV methods. When possible, a second strategy to reduce the number of unknowns consists in solving the discrete problems in terms of face unknowns only, see the discussion in [6]. The linear systems resulting from VLO discretizations can be solved efficiently with standard preconditioners when mild homogeneities are present. Unlike MPFV methods, the embedded stability ensures that the matrices are definite;

– local conservation. When interface unknowns are kept, the local conservation properties of VLO methods can be formulated in terms of numerical fluxes whose expression can be obtained analytically. In this case, the interface unknowns act as Lagrange multipliers of the flux continuity constraint. For further details we refer [6, 18];
– integrability into existing simulators. Even when a simple expression for the numerical flux is available, VLO methods are less easily integrated into existing numerical codes when compared to MPFV methods. Indeed, dealing with interface unknowns, whether they are kept or interpolated, may require substantial modifications of the data structures and of the way parallelism is handled.

2.5 Discontinuous Galerkin Methods

2.5.1 Principles

The key idea of dG methods is to search the approximate solution in a space of piecewise polynomial functions that are fully discontinuous at interfaces, *i.e.*, for an integer $k \geq 1$:

$$V_h^k := \left\{ v \in L^2(\Omega) \,|\, v_{|T} \in \mathbb{P}_d^k(T),\ \forall T \in \mathcal{T}_h \right\}$$

where $\mathbb{P}_d^k(T)$ denotes the restriction to T of polynomial functions of total degree $\leq k$. The main advantage of considering fully discontinuous functions is that sharp gradients or singularities affect the numerical solution only locally, which is not the case when considering discrete spaces endowed with some form of global regularity. This feature was first recognized in 1973 [62], who introduced a dG discretization of a steady neutron transport problem. The first analysis for steady first-order PDE is due to Lesaint and Raviart [63-65]. However, dG methods only reached popularity in the 90s, when Cockburn and Shu considered their application to time-dependent hyperbolic PDE in conjunction with explicit Runge-Kutta schemes [66, 67]. For PDE with diffusion, dG methods originate from the work of Nitsche on boundary-penalty methods in the early 70s [68, 69] and the use of Interior Penalty (IP) techniques to weakly enforce continuity conditions imposed on the solution or its derivatives across interfaces [59, 70-72]. In the late 90s, following the success of Runge-Kutta dG methods applied to hyperbolic problems, a new interest arose in dG formulations of diffusion terms. An extension of the techniques of Cockburn and Shu to problems with diffusion was considered [73] in the context of compressible flows. A unified analysis of dG methods for diffusive terms can be found in the work of Arnold *et al.* [74], while a unified analysis encompassing both diffusive and hyperbolic PDE has been derived [75-77].

The use of dG methods in geosciences has been considered in several works, mainly focusing on reactive transport, where advection terms play an important role; cf., *e.g.*, Sun and Wheeler [78, 79] or Bastian *et al.* [80] and references therein. In this context, a key point is to ensure the robustness of the method in the vanishing or zero permeability limit. This problem has been addressed by Houston *et al.* [81], and Di Pietro *et al.* [7]. The latter work provides the backbone for the discussion in the following section.

2.5.2 Degenerate Advection-Diffusion

Following [7], we show how the features of dG methods can be exploited to construct a discretization which is robust with respect to vanishing (or even zero) permeability. We modify (2) to include advection and reaction terms:

$$\begin{aligned} \boldsymbol{\nabla} \cdot (-\mathbf{K}\boldsymbol{\nabla} u + \boldsymbol{\beta} u) + \mu u = f \ \text{ in } \ \Omega \\ u = 0 \ \text{ on } \ \partial\Omega^* \end{aligned} \qquad (19)$$

where $\boldsymbol{\beta}$ is an incompressible vector-valued velocity field, $\mu > 0$ is a reaction coefficient, while:

$$\partial\Omega^* := \{ \boldsymbol{x} \in \partial\Omega \,|\, (\mathbf{K}\boldsymbol{n} \cdot \boldsymbol{n})(\boldsymbol{x}) > 0 \text{ or } \beta \cdot n < 0 \} \qquad (20)$$

($\boldsymbol{n}$ denotes here the unit normal vector pointing out of Ω). To include the case when the permeability tensor vanishes along one direction, the boundary condition is only enforced on the portion of $\partial\Omega$ where either normal diffusion is present, or where the advective flow enters the domain. Problem (19) is representative of a class of reactive transport models encountered, *e.g.*, in CO_2 storage simulation. It has been shown in [7] that the solution to (19) features singularities along the discontinuities of the permeability field. In particular, jumps occur when the advection field flows from a non-permeable to a permeable region, as shown in Figure 6. Jump singularities are not naturally handled by methods such as the ones described in Section 2.4.2, since the gradient reconstruction (9) is inherently based on the approximation of single-valued traces. On the contrary, discontinuities can be captured by dG methods provided they occur at element boundaries and not inside elements. To make sure that the appropriate interface conditions are automatically selected:
– diffusive penalization of interface jumps should only occur when the permeability in the normal direction is nonzero on both sides of an interface. This is the

case, *e.g.*, for the bilinear form a_h^{swip}, where the harmonic averaging in (16) makes the penalty term vanish if $\lambda_1\lambda_2 = 0$;
- advective penalization of interface jumps should incorporate a mechanism to enforce boundary conditions on the inflow portion of $\partial\Omega^*$ and interface condition on the interface between permeable and nonpermeable regions.

It has been shown in [7] that this is the case when upwind fluxes are considered, corresponding to the bilinear form:

$$a_h^{\mathrm{upw}}(u_h, v_h) := -\int_\Omega u_h(\boldsymbol{\beta}\cdot\boldsymbol{\nabla}_h v_h) + \sum_{F\in\mathcal{F}_h}\int_F \Phi_h^{\mathrm{upw}}(u_h)[\![v_h]\!]$$

where, letting $\beta_F := \boldsymbol{\beta}\cdot\boldsymbol{n}_F$ for all $F\in\mathcal{F}_h$ and setting, for a real x, $x^{\oplus} := 1/2(|x|+x)$:

$$\Phi_h^{\mathrm{upw}}(u_h) := \begin{cases} \beta_F\{u_h\} + \frac{1}{2}|\beta_F|[\![u_h]\!] & \text{if } F\in\mathcal{F}_h^{\mathrm{i}} \\ \beta_F^{\oplus}u_h & \text{if } F\in\mathcal{F}_h^{\mathrm{b}} \end{cases}$$

The discretization of problem (19) reads:
Find $u_h\in V_h^k$ such that, for all $v_h\in V_h^k$:

$$a_h^{\mathrm{swip}}(u_h, v_h) + a_h^{\mathrm{upw}}(u_h, v_h) + \int_\Omega \mu u_h v_h = \int_\Omega f v_h \qquad (21)$$

An important difference with respect to the methods of Section 2.4.2 is that, this time, the discrete problem is formulated for an arbitrary order $k \geq 1$. As an example, convergence results for the problem described in Figure 6 are provided in Figure 7.

2.5.3 Discussion

We briefly revise the features of dG methods with respect to the points identified in Section 2.1:
- consistency. Since dG methods are (nonconforming) finite element methods, consistency can be interpreted as an orthogonality property for the numerical error $u - u_h$. This has the important consequence that higher-order approximations can be considered, since the convergence rate is not limited by the consistency error. The use of high-order methods in subsoil modeling, although not common, can be justified when complex flow patterns are present [82];
- robustness. As shown in the previous section, it is possible to design dG methods that are robust with respect to variations of the physical parameters of the problem. Indeed, the additional flexibility resulting from the use of fully discontinuous polynomial

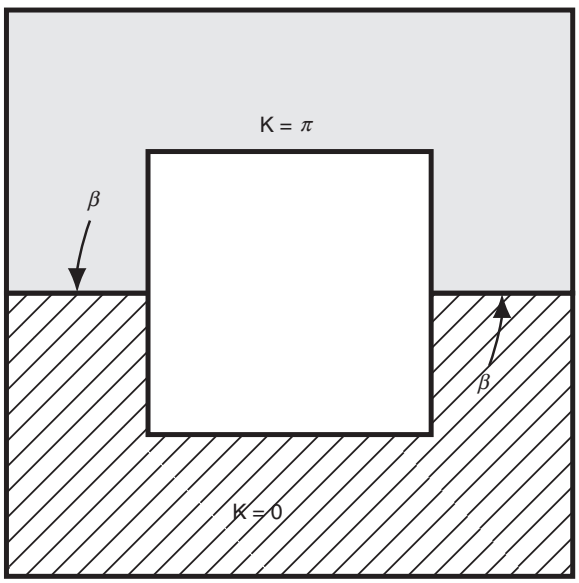

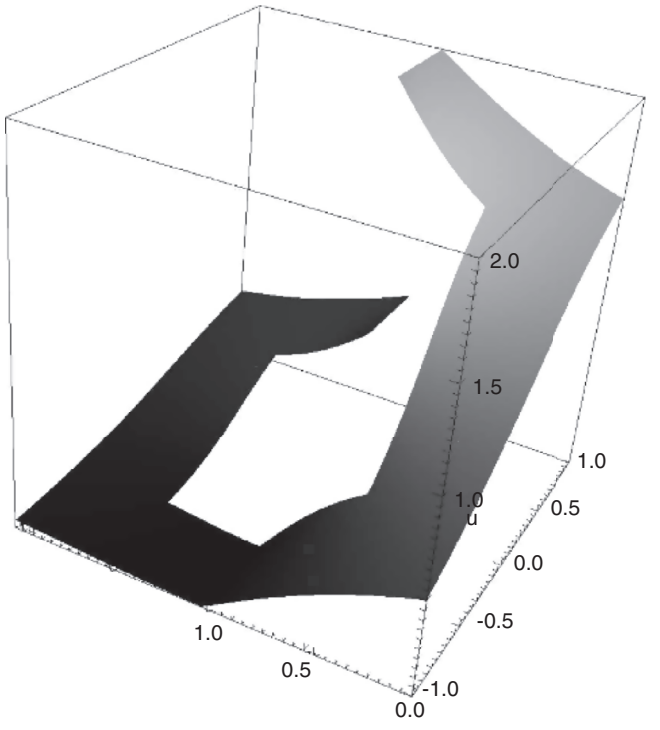

Figure 6

Jumps singularity occurring when the advection field $\boldsymbol{\beta}$ flows from a nonpermeable (etched) to a permeable (shaded) region.

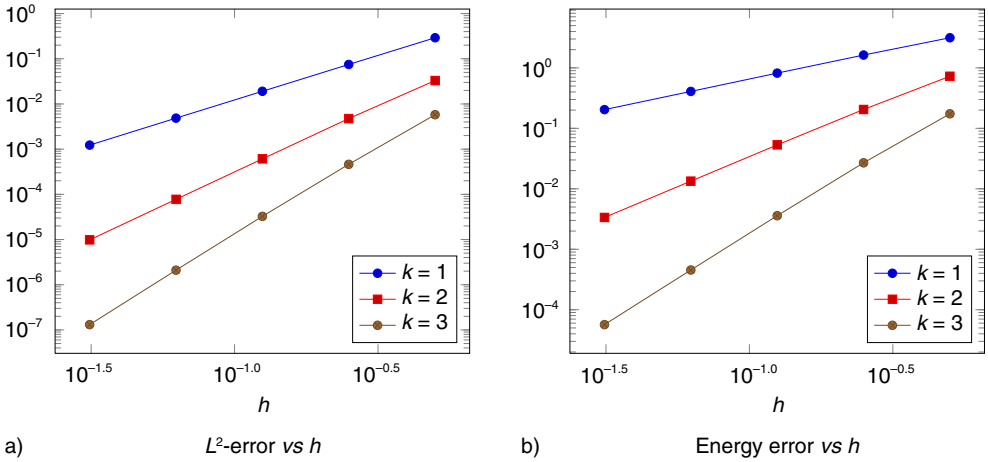

Figure 7

Convergence of the dG method (21) for the problem of Figure 6.

spaces allows to represent singularities in the solution which would otherwise affect the overall precision. More generally, coarse features can be expected to have only local effects, leaving the numerical solution in the far field unperturbed;

- stability. The stability of dG method is inherent to the use of penalty terms which allow to control the jumps of the discrete solution at interfaces. A relevant point in the example of Section 2.5.2 is that these terms can be finely tuned to avoid unnecessary (or unphysical) numerical diffusion. As is the case for all of MPFA and VLO methods, the discrete maximum principle is not available in general;
- low computational cost. Discontinuous Galerkin methods are usually the most expensive among the methods considered in this review. In fact, a fully discontinuous polynomial representation requires to introduce as many cell DOFs as the coefficients of a polynomial in $\mathbb{P}_d^k$. Moreover, the resulting linear systems are usually more difficult to solve, although standard preconditioners are still usable when mild heterogeneities are present;
- local conservation. Although this point is not detailed here for the sake of conciseness, it has been long known that dG methods enjoy local conservation properties expressed in terms of continuous numerical fluxes [20-22, 74];
- integrability into existing simulators. Discontinuous Galerkin methods are generally difficult to integrate into existing finite volume codes, while this is generally easier for finite element codes. One point in favor of dG methods is that the connectivity is analogous to that of the TPFV method, which therefore can be used as a model to design communications in parallel implementations.

3 *A POSTERIORI* ERROR ANALYSIS AND ADAPTIVE ALGORITHMS

This last section of our paper is devoted to *a posteriori* error estimates and adaptive algorithms for the considered problems in geosciences. The use of *a posteriori* estimates enables to control the error and *a posteriori*-driven algorithms appear as a promising way of compensating the increased computational cost for complex models. Recently, the *a posteriori* theory has advanced considerably and is now available for most of the discretization methods discussed in Section 2. Moreover, this theory has been unified such that it can be presented independently of the particular numerical discretization. We use such a spirit here, while following the recent contributions [27, 83-93]. The basic idea of this approach can be traced back at least to the Prager and Synge equality [94] and has been used in *a posteriori* error estimation from the 70s; we refer for a general orientation to the monographs [23, 95-98] and for milestone contributions [24-26, 99-105]. For a general orientation in error components distinction and adaptive nonlinear and linear solvers [106-109]. Rather engineering approaches have also been previously proposed; let us in particular refer to [2].

3.1 General Considerations

A posteriori error estimates aim at giving bounds on the error between the known numerical approximation, say

$u_{h\tau}$, and the unknown exact solution, say u, that can be computed in practice, once the approximate solution $u_{h\tau}$ is known. They typically take the form:

$$|||u - u_{h\tau}||| \leq \left\{ \sum_{n=1}^{N} \sum_{T \in \mathcal{T}_h^n} (\eta_T^n)^2 \right\}^{\frac{1}{2}} \tag{22}$$

where $\eta_T^n = \eta_T^n(u_{h\tau})$ is a quantity linked to the discrete time t^n and mesh element T, computable from $u_{h\tau}$, called an *element estimator*. In (22), $|||\cdot|||$ is some space-time error measure, like the energy norm. Estimate (22) is written directly for an unsteady problem; for steady problems, we simply set $N := 1$ and leave out the temporal indices n. Then, $|||\cdot|||$ is only a space error measure and we use the notation u_h for the approximate solution. Detailed notation is given below.

One may formulate the following six properties to describe an optimal *a posteriori* error estimate:

(i) ensure that (22) holds and that the element estimators η_T^n are fully computable from $u_{h\tau}$ (guaranteed upper bound);

(ii) ensure that, for all $1 \leq n \leq N$ and all $T \in \mathcal{T}_h^n$, η_T^n represents a lower bound for the actual error on the time interval $(t^{n-1}, t^n]$ and in the vicinity of the element T, up to a generic constant; this means that there exists a constant $C > 0$ such that:

$$\eta_T^n \leq C|||u - u_{h\tau}|||_{(t^{n-1},t^n] \times \mathfrak{T}_T} \tag{23}$$

where $\mathfrak{T}_T$ stands for the element T and its neighbors (local efficiency);

(iii) ensure that the effectivity index defined as the ratio of the estimated and actual error:

$$I_{\mathit{eff}} := \frac{\left\{ \sum_{n=1}^{N} \sum_{T \in \mathcal{T}_h^n} (\eta_T^n)^2 \right\}^{\frac{1}{2}}}{|||u - u_{h\tau}|||} \tag{24}$$

goes to one as the computational effort grows (asymptotic exactness);

(iv) guarantee the three previous properties independently of the parameters of the problem and of their variations (robustness);

(v) give estimators η_T^n which can be evaluated locally (only performing calculations in the element T or in its neighborhood $\mathfrak{T}_T$ and on the time levels $n-1$, n, $n+1$) (small evaluation cost);

(vi) distinguish and estimate separately the different error components (error components identification).

Property (i) above allows to give a truly computable upper bound on $|||u - u_{h\tau}|||$ and thus to certify the error committed in a numerical simulation. Property (ii) enables to predict the localization of the error. It is possible to satisfy it entirely for steady problems. It then enables to detect the areas of the computational domain Ω where the error is large. Knowing such areas, one can concentrate more effort therein, by performing an adaptive mesh refinement. For unsteady problems, one typically only arrives at:

$$\left\{ \sum_{T \in \mathcal{T}_h^n} (\eta_T^n)^2 \right\}^{1/2} \leq C|||u - u_{h\tau}|||_{(t^{n-1},t^n]} \tag{25}$$

in place of (23). This justifies theoretically the localization of the error in time but not in space. Property (iii) ensures the optimality of the upper bound; if the error is quite small and the estimator predicts a large value, it may satisfy properties (i) and (ii), but is probably not very useful as it significantly overestimates the error. Property (iv) is one of the most important in practice. In real-life problems, parameters and coefficients such as the size of the computational domain Ω, the final simulation time t_F, space and time steps h and τ, the permeability tensor $\mathbf{K}$, the porosity ϕ, the viscosities μ, the sources q, and the nonlinear state functions for nonlinear problems may be very large or small or vary abruptly; an estimator satisfying property (iv) ensures that its results will be equally good in all possible situations. Property (v) then guarantees that the computational cost needed for the evaluation of the estimators η_T^n will be much smaller than the cost required to obtain the approximate solution $u_{h\tau}$ itself (recall that typically a global problem needs to be solved in order to obtain the approximate solution for steady problems and one such a problem needs to be solved at each time step for implicit time discretizations of unsteady problems). Finally, the numerical error $u - u_{h\tau}$ typically consists of several error components. The first one is the discretization error, which further splits into temporal (for unsteady problems) and spatial errors. These result from the approximation properties of the time stepping procedure and of the numerical scheme, and from the current temporal and spatial meshes. Another typical error component is the algebraic error, linked to the imprecision in the solution of the associated systems of linear algebraic equations. For nonlinear problems, the linearization error, linked to incomplete convergence of iterative nonlinear solvers such as the Newton method, arises equally. Property (vi) is essential for the identification of the discretization (spatial and temporal), linearization, and algebraic errors and for entire adaptivity, relying not solely on adaptive mesh refinement but employing crucially adaptive stopping criteria for linear and nonlinear solvers.

In the subsequent sections, we will illuminate the current knowledge on *a posteriori* error estimates for problems in geosciences. We start by the model steady linear problem

(2) and arrive up to the compositional Darcy flow model discussed in Section 1. The error estimates are derived under very general assumptions that allow to cover all the discretization methods discussed in Section 2, taking advantage of the unified framework developed in [27, 86, 87, 88, 92], see also the references therein.

3.2 Single-Phase Steady Darcy Flow

Let us first consider the single-phase Darcy flow (2). In order to make the presentation independent of the numerical scheme at hand, we suppose that u_h is piecewise regular, typically a piecewise polynomial function on the mesh $\mathcal{T}_h$. This in particular allows for u_h being nonconforming, *i.e.*, not contained in the energy space $H^1_0(\Omega)$.

3.2.1 Controlling *a Posteriori* the Error

To give an *a posteriori* error estimate for the generic approximation u_h we follow [87, 88, 90, 92]; henceforth we assume that we are able to construct two functions s_h and $\boldsymbol{\sigma}_h$ such that:

Assumption 1 (Potential reconstruction)

There exists a scalar function $s_h \in H^1_0(\Omega)$, *termed* potential reconstruction.

Assumption 2 (Equilibrated flux reconstruction)

There exists a vector function $\boldsymbol{\sigma}_h \in \mathbf{H}(\mathrm{div}, \Omega)$ *such that*:

$$(\nabla \cdot \boldsymbol{\sigma}_h, 1)_T = (f, 1)_T \quad \forall T \in \mathcal{T}_h$$

termed equilibrated flux reconstruction.

The two above assumptions mimic two essential properties of the exact solution of (2). First, since the exact pressure u belongs to the space $H^1_0(\Omega)$, its jumps across interfaces vanish as detailed, *e.g.*, in [22, Lemma 1.23], and its trace on $\partial\Omega$ is zero. Second, the exact (Darcy) flux given by $-\mathbf{K}\nabla u$ belongs to the space $\mathbf{H}(\mathrm{div}, \Omega)$, which implies, in particular, that its normal component is continuous across interfaces in a proper sense. Last, for the exact flux it holds that its divergence is equal to the source term f. Assumptions 1 and 2 mimic these properties on the discrete level. In conforming numerical methods such as vertex-centered FV or conforming FE, the approximate solution itself satisfies $u_h \in H^1_0(\Omega)$. Then, we simply set $s_h := u_h$. Otherwise, s_h satisfying Assumption 1 is chosen as close as possible to u_h. Similarly, in flux-conforming numerical methods such as cell-centered FV or mixed finite elements, a discrete flux satisfying Assumption 2 is readily available and can be taken for $\boldsymbol{\sigma}_h$. Otherwise, $\boldsymbol{\sigma}_h$ satisfying Assumption 2 is chosen as close as possible to $-\mathbf{K}\nabla_h u_h$.

Suppose $f \in L^2(\Omega)$, $\mathbf{K}$ symmetric, bounded, and uniformly positive definite, and recall that the energy norm for problem (2) is defined as $|||v||| := ||\mathbf{K}^{1/2}\nabla v||_{L^2(\Omega)^d}$. For functions v only piecewise H^1 on the mesh $\mathcal{T}_h$, we extend it to a semi-norm by setting $|||v||| := ||\mathbf{K}^{1/2}\ \nabla_h v||_{L^2(\Omega)^d}$. Then we have, see [87, 90, 92, 94]

Theorem 1 *A posteriori* error estimate, steady single phase flow

Let u be the exact (weak) solution of (2), *let u_h be its arbitrary (piecewise regular) approximation, and let Assumptions 1 and 2 hold. Then:*

$$|||u - u_h||| \le \left\{ \sum_{T \in \mathcal{T}_h} (\eta_{\mathrm{F},T} + \eta_{\mathrm{R},T})^2 + \sum_{T \in \mathcal{T}_h} \eta^2_{\mathrm{NC},T} \right\}^{1/2}$$

where the nonconformity estimators $\eta_{\mathrm{NC},T}$ are given by:

$$\eta_{\mathrm{NC},T} := ||\mathbf{K}^{1/2}\nabla_h(u_h - s_h)||_T$$

the flux estimators $\eta_{\mathrm{F},T}$ are given by:

$$\eta_{\mathrm{F},T} := ||\mathbf{K}^{1/2}\nabla_h u_h + \mathbf{K}^{-1/2}\boldsymbol{\sigma}_h||_T$$

and the residual estimators $\eta_{\mathrm{R},T}$ are given by:

$$\eta_{\mathrm{R},T} := \frac{C_{\mathrm{P},T} h_T}{c^{1/2}_{\mathbf{K},T}} ||f - \nabla \cdot \boldsymbol{\sigma}_h||_T$$

In Theorem 1, $C_{\mathrm{P},T}$ is the constant from the Poincaré inequality, equal to $1/\pi$ whenever the element T is convex, and $c_{\mathbf{K},T}$ is the smallest eigenvalue of the permeability tensor $\mathbf{K}$ on the element T.

Remark 1 (Estimators of Theorem 1)

The estimator $\eta_{\mathrm{NC},T}$ of Theorem 1 is related to the $H^1_0(\Omega)$-*constraint* on the pressures and evaluates the possible departure of u_h from $H^1_0(\Omega)$. The estimator $\eta_{\mathrm{F},T}$ is related to *constitutive law* saying that the flux is given by $-\mathbf{K}\nabla u$ (this is precisely the Darcy law (1b) when the gravitational effects are neglected) and to the $\mathbf{H}(\mathrm{div}, \Omega)$-*constraint* on the fluxes and evaluates the departure of $-\mathbf{K}\nabla_h u_h$ from $\mathbf{H}(\mathrm{div}, \Omega)$. Finally, the last estimator $\eta_{R,T}$ is related to the strong form (2) and to the condition of flux being in *equilibrium* with the sources.

It follows from Theorem 1 that the *a posteriori* estimate for the energy norm of the approximation error for problem (2) is certified, so that property (i) of Section 3.1 is satisfied. With appropriate choices of the reconstructions s_h and $\boldsymbol{\sigma}_h$, it can be shown that also the properties (ii)-(v) hold true; property (iii) may not hold fully (but effectivity indices below two are usually observed), and, similarly, property (iv) does generally not hold with respect to the heterogeneities and anisotropies of the diffusion tensor $\mathbf{K}$. More precisely, robustness with respect to heterogeneities do holds whenever a path

with monotonous growth of the diffusivity around each node exists [110, Hypothesis 2.7]. This monotonicity assumption is not necessary for schemes using harmonic averaging and dual meshes [91] and the discussion therein. Robustness with respect to anisotropies typically does not hold for the energy (semi-)norm but may hold for other (weaker) norms [91, Remark 5.9]. Finally, the estimate of Theorem 1 assumes that the system of linear equations associated to the given numerical method is solved exactly. Identification of the algebraic and discretization errors in the spirit of property (vi), leading to stopping criteria for iterative liner solvers, was undertaken in [89] and in a broader setting in [27]. Details with in particular the constructions of s_h and $\boldsymbol{\sigma}_h$ for various numerical methods can be found in [87, 90, 92].

3.2.2 Refining Adaptively the Mesh

If follows from the fact that property (ii) of Section 3.1 is satisfied that the estimators of Theorem 1 allow us to predict the spatial distribution of the error. This is illustrated in Figure 8a, where the estimators for the cell-centered TPFV scheme approximation of (2) are shown, whereas in Figure 8b, the actual error distribution over the mesh elements is plotted. We can see that our prediction matches nicely the reality. It is then natural to refine the mesh adaptively, around those elements where the estimators predict a high error value. Such a concept is crucial especially in presence of singularities in the exact solution: then the mesh can be almost exclusively refined in such places, as we can witness it in Figure 9. Both these examples, as well as the one in Figure 10, are given for problem (2) with a model domain $\Omega = (-1, 1) \times (-1, 1)$, zero source term f, isotropic but inhomogeneous diffusion tensor $\mathbf{K}$ being ϵ multiple of the identity tensor in the first and third quadrant and by the identity tensor in the two remaining quadrants, and with an inhomogeneous Dirichlet boundary condition instead of the homogeneous one. This problem admits an analytical solution featuring a singularity at the origin [90]. We consider two cases $\epsilon = 5$ and $\epsilon = 100$ corresponding to Figure 8 and Figure 9, respectively.

Finally, in Figure 10, we first asses the precision of our estimators: we plot both the energy error $|||u - u_h|||$ and the estimate of Theorem 1, for $\epsilon = 5$ (*Fig. 10a*) and for $\epsilon = 100$ (*Fig. 10b*). We see that our estimators overestimate the actual error only mildly. Second, Figure 10 compares the situation of classical uniform mesh refinement with the adaptive mesh refinement based on our estimators. We see that the same precision can be achieved for significantly fewer unknowns in the adaptive case with respect to the uniform one. Equivalently, the error for the same number of unknowns is much smaller in the adaptive case. Actually, the error decrease in function of the number of unknowns is very slow (owing to the low regularity of the solution) in the uniform case, whereas it recovers the best possible speed in the adaptive case [90].

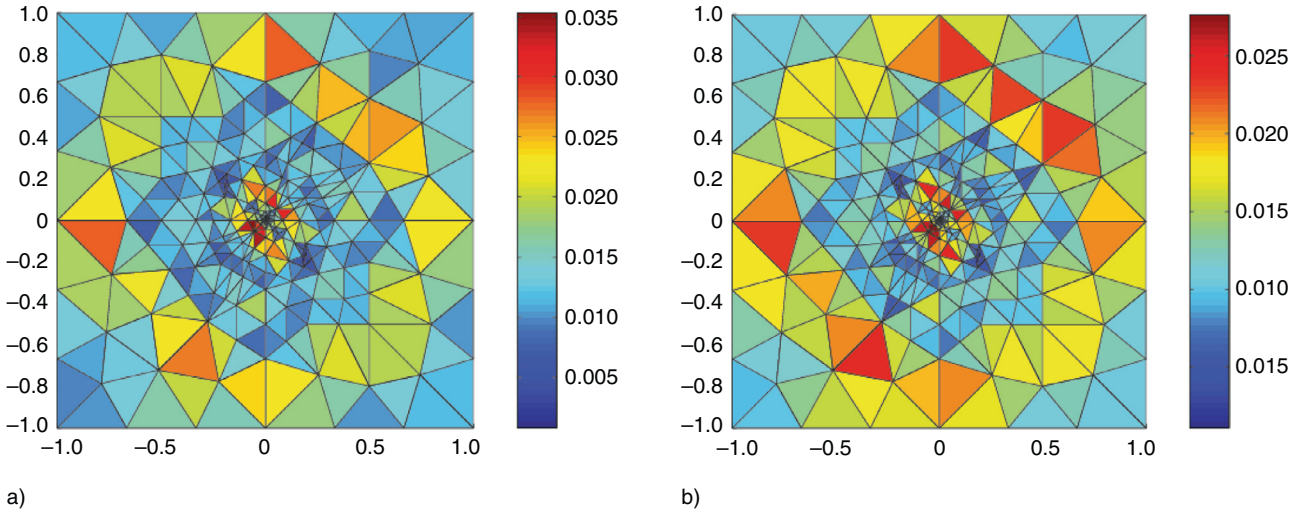

Figure 8

Estimated (a) and actual (b) error distribution, permeability ratio 1:5, single-phase steady Darcy flow. The pictures are taken from reference [90].

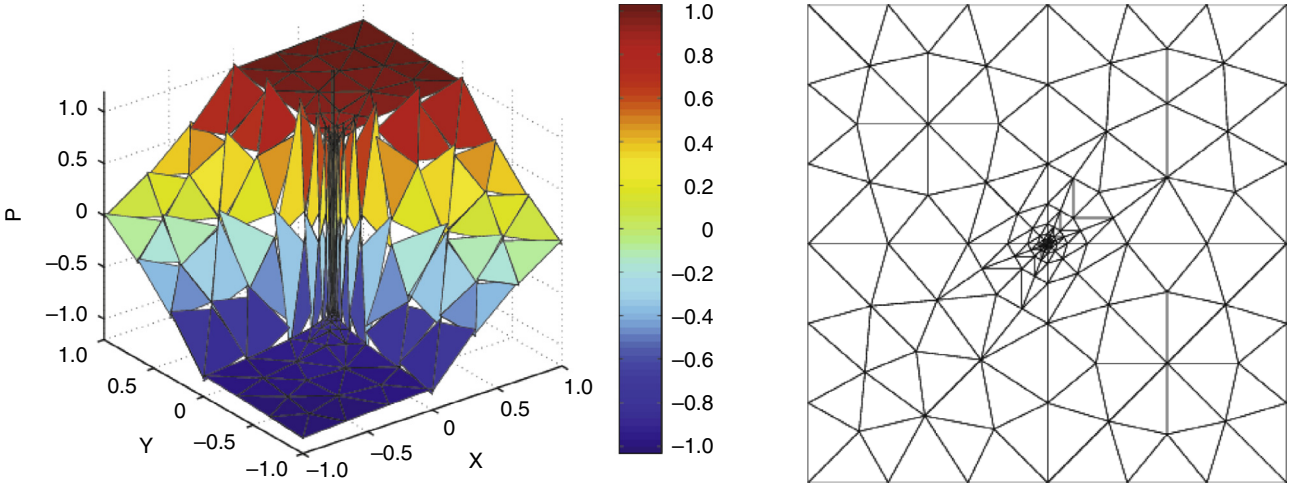

Figure 9

Approximate solution and the corresponding adaptively refined mesh, permeability ratio 1:100, single-phase steady Darcy flow. The pictures are taken from reference [90].

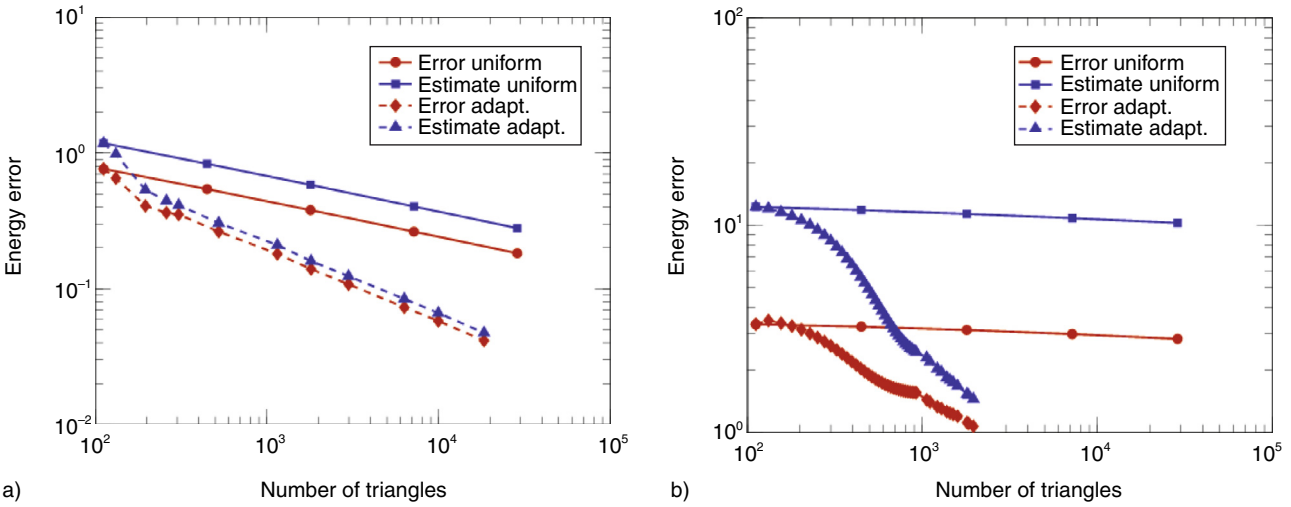

Figure 10

Estimated and actual error against the number of elements in uniformly/adaptively refined meshes for permeability ratio a) 1:5 and b) 1:100, single-phase steady Darcy flow. The pictures are taken from reference [90].

3.3 Single-Phase Unsteady Darcy Flow

To lay the foundations for time-dependent problems, we consider the unsteady version of the model problem (2). For the sake of simplicity, we take for the theoretical developments $\mathbf{K}$ to be the identity matrix, so that we look for u such that:

$$\begin{aligned} \partial_t u - \nabla \cdot (\nabla u) &= f \quad \text{in } \Omega \times (0, t_F) \\ u &= 0 \quad \text{on } \partial\Omega \times (0, t_F) \\ u(\cdot, 0) &= u_0 \quad \text{in } \Omega \end{aligned} \tag{26}$$

for some given initial pressure u_0. Let t^n, $0 \le n \le N$, be a strictly increasing sequence of discrete times such that $t^0 = 0$ and $t^N = t_F$. We introduce the time intervals $I_n := (t^{n-1}, t^n]$ and the time steps $\tau^n := t^n - t^{n-1}$ for all $1 \le n \le N$. On each t^n, we suppose a (possibly different) mesh $\mathcal{T}_h^n$. Again, to make the presentation as general as possible, and to include all the space discretization schemes discussed in Section 2, we suppose that $u_{h\tau}$ is such that $u_h^n := u_{h\tau}(\cdot, t^n)$ is piecewise regular (typically piecewise polynomial) on $\mathcal{T}_h^n$, and that $u_{h\tau}$ is continuous and piecewise affine with respect to time. We assume the

temporal discretization that is fully implicit, backward Euler. We follow in our presentation [86, 87, 92].

3.3.1 Controlling *a Posteriori* the Error

Let the source function $f \in L^2(\Omega \times (0,t_F))$ be for simplicity piecewise constant in time, where we denote $f^n := f|_{I_n}$, and let the initial condition $u_0 \in L^2(\Omega)$. The exact solution lies in the space $Y := \{y \in X; \partial_t y \in X'\}$, with $X := L^2(0,t_F;H_0^1(\Omega))$ and $X' = L^2(0,t_F;H^{-1}(\Omega))$. The space-time energy norm is given by, for $y \in X$:

$$||y||_X := \left\{ \int_0^{t_F} ||\nabla y||^2(t)\mathrm{d}t \right\}^{1/2} \tag{27}$$

We extend it to only piecewise regular functions in space while replacing the usual gradient ∇ by the broken one ∇_h. It appears impossible so far to obtain (23) or (25) from property (ii) for the energy norm (27). For this reason, we [102], augment the energy norm by a dual norm of the time derivative as:

$$||y||_Y := ||y||_X + ||\partial_t y||_{X'} \tag{28}$$

with:

$$||\partial_t y||_{X'} := \left\{ \int_0^{t_F} ||\partial_t y||^2_{H^{-1}}(t)\mathrm{d}t \right\}^{1/2}$$

Then, property (ii) (the local in time but global in space version (25)) can be obtained.

We make the following equivalents of Assumptions 1 and 2:

Assumption 3 (Potential reconstruction)

There exists a scalar function $s_{h\tau}$, continuous and piecewise affine in time and satisfying $s_h^n := s_{h\tau}(\cdot,t^n) \in H_0^1(\Omega)$, such that, for all $1 \le n \le N$ and for all $T \in \mathcal{T}_h^n$:

$$(\partial_t s_{h\tau}^n, 1)_T = (\partial_t u_{h\tau}^n, 1)_T \tag{29}$$

where $s_{h\tau}^n := s_{h\tau}|_{I_n}$ and $u_{h\tau}^n := u_{h\tau}|_{I_n}$. We call $s_{h\tau}$ a potential reconstruction.

Remark 2 (Condition (29))

Condition (29) is necessary as we shall estimate the error in the augmented $||\cdot||_Y$-norm of (28). For a similar estimate in the $||\cdot||_X$-norm of (27), it would not be necessary.

Assumption 4 (Equilibrated flux reconstruction)

There exists a vector function $\boldsymbol{\sigma}_{h\tau}$, piecewise constant in time, such that, for all $1 \le n \le N$, $\boldsymbol{\sigma}_h^n := \boldsymbol{\sigma}_{h\tau}|_{I_n} \in \mathbf{H}(\mathrm{div},\Omega)$ and:

$$(f^n - \partial_t u_{h\tau}^n - \nabla \cdot \boldsymbol{\sigma}_h^n, 1)_T = 0 \quad \forall T \in \mathcal{T}_h^n$$

We call $\boldsymbol{\sigma}_{h\tau}$ an equilibrated flux reconstruction.

We then have [86, 87, 92]:

Theorem 2 (*A posteriori* error estimate, unsteady single phase flow)

Let u be the exact (weak) solution of (26) and let $u_{h\tau}$ be its arbitrary piecewise regular in space and continuous and piecewise affine in time approximation. Let Assumptions 3 and 4 be satisfied. Then:

$$||u - u_{h\tau}||_Y \le \left\{ \sum_{n=1}^N (\eta_{\mathrm{sp}}^n)^2 \right\}^{\frac{1}{2}} + \left\{ \sum_{n=1}^N (\eta_{\mathrm{tm}}^n)^2 \right\}^{\frac{1}{2}} + \eta_{\mathrm{IC}} \tag{30}$$

with, for all $1 \le n \le N$, the spatial and temporal error estimators given respectively by:

$$(\eta_{\mathrm{sp}}^n)^2 := \sum_{T \in \mathcal{T}_h^n} 3\{\tau^n (9(\eta_{\mathrm{R},T}^n + \eta_{\mathrm{F},T}^n)^2 + (\eta_{\mathrm{NC},2,T}^n)^2) + \int_{I_n} (\eta_{\mathrm{NC},1,T}^n)^2(t)\,\mathrm{d}t\}$$

$$(\eta_{\mathrm{tm}}^n)^2 := \sum_{T \in \mathcal{T}_h^n} 3\tau^n ||\nabla(s_h^n - s_h^{n-1})||_T^2$$

For all $T \in \mathcal{T}_h^n$, the residual estimator, the flux estimator, and the nonconformity estimators are given respectively by:

$$\eta_{\mathrm{R},T}^n := C_{\mathrm{P},T} h_T ||f^n - \partial_t s_{h\tau}^n - \nabla \cdot \boldsymbol{\sigma}_h^n||_T$$

$$\eta_{\mathrm{F},T}^n := ||\nabla s_h^n + \boldsymbol{\sigma}_h^n||_T$$

$$\eta_{\mathrm{NC},1,T}^n(t) := ||\nabla_h (s_{h\tau} - u_{h\tau})(t)||_T, \forall t \in I_n$$

$$\eta_{\mathrm{NC},2,T}^n := C_{\mathrm{P},T} h_T ||\partial_t (s_{h\tau} - u_{h\tau})^n||_T$$

Finally, the initial condition estimator is given by:

$$\eta_{\mathrm{IC}} := 2^{1/2} ||s_h^0 - u_0||$$

It follows from Theorem 2 that the augmented norm error (28) in approximation of problem (26) is certified by the *a posteriori* error estimate (30), so that property (i) of Section 3.1 is satisfied. With appropriate choices of the reconstructions $s_{h\tau}$ and $\boldsymbol{\sigma}_{h\tau}$, it can be shown that property (ii), with (25) in place of (23), holds true (the efficiency is local in time but unfortunately only global in space as discussed in Sect. 3.1). Concerning property (iii), it typically only gives effectivity indices around five. Finally, all properties (iv)-(vi) hold true. It is important that property (iv) does hold with respect to the final time t_F, so that the overestimation factor does not depend on the length of the simulation. Finally, as stipulated by property (vi), the estimators η_{sp}^n and η_{tm}^n decompose the

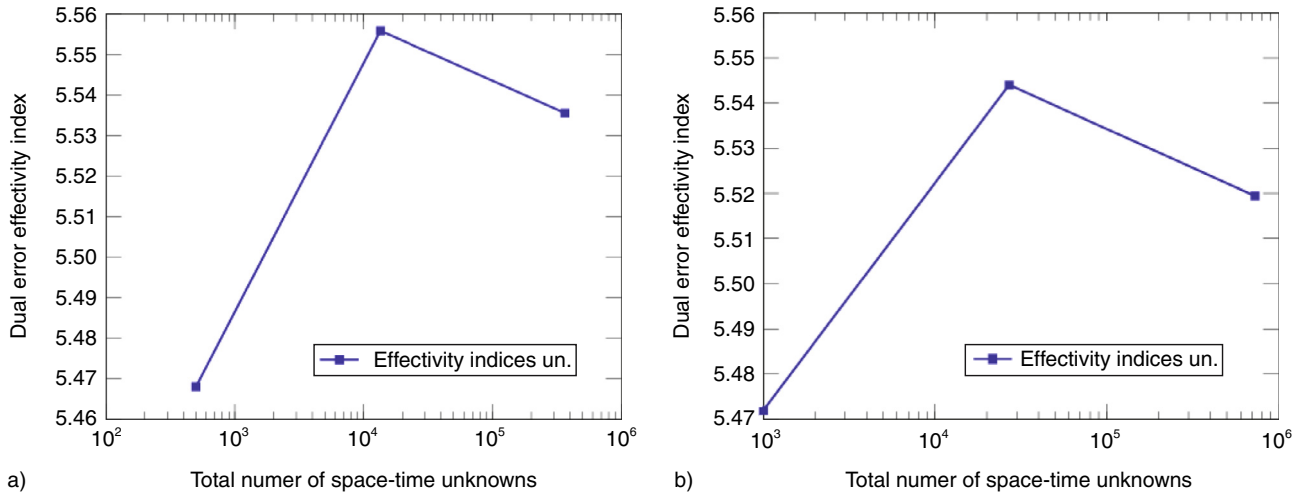

Figure 11

Effectivity indices for final times a) $t_F = 1.5$ and b) $t_F = 3$, augmented norm error $||u - u_{h\tau}||_Y$, single-phase unsteady Darcy flow.

error into its two components, the spatial and temporal ones.

In Figure 11, we give a numerical illustration of the robustness with respect to the final time t_F. We consider problem (26) posed on the domain $\Omega := (0,3) \times (0,3)$ with $\mathbf{K} = 0.5\mathbb{I}$ ($\mathbb{I}$ being the identity matrix), $f = 0$, and with u_0 and an inhomogeneous Dirichlet boundary condition given by the exact solution $u(\boldsymbol{x},t) = \frac{e^x e^y e^t}{e^3}$. Three square meshes of Ω with 10×10, 30×30, 90×90 grids and associated time steps 0.3, 0.1, 0.03333 are considered. A vertex-centered finite volume scheme with backward Euler time stepping is tested in Figure 11a for $t_F = 1.5$ and in Figure 11b for $t_F = 3$. The results confirm experimentally that the effectivity indices are independent of the final time. For illustration, we give the effectivity indices also for the energy norm (27) and appropriately modified estimators in Figure 12. Although in this case we have no theoretical support, we numerically observe efficiency and the same robustness with respect to the final time; moreover, here the effectivity indices are closer to the optimal value of one.

3.3.2 Adaptivity: Mesh and Time Step (De)refinement

The distinction of the spatial and temporal error components of Theorem 2 is a basic theoretical ingredient for adaptivity in unsteady problems, where both the spatial meshes $\mathcal{T}_h^n$ and the time steps τ^n can be refined and derefined during the simulation. An example of a resulting adaptive algorithm and numerical illustrations of the computational benefits of such a space-time adaptive approach can be found in [111], see also Algorithm 1 below.

3.4 The Two-Phase Unsteady Darcy Flow

We now move in our presentation further to the simplest multi-phase flow model: we consider a simplification of the compositional model of Section 1 with only two phases present and one component identified with each phase. The results of Sections 3.2 and 3.3 were recently extended to such a case in [83] for vertex-centered finite volume discretizations and in [93] in a general, discretization scheme-independent setting, developing the ideas of [27, 85, 86, 89]. We focus here particularly on property (vi) from Section 3.1 and on its practical benefits; all the mathematical details can be found in [83, 93].

3.4.1 Controlling *a Posteriori* the Error

Suppose again an implicit Euler time discretization. In analogy with Sections 3.2 and 3.3, to give an *a posteriori* error estimate for general approximations $(S_{p,h\tau}, P_{p,h\tau})$, $p \in \mathcal{P}$ fixed, without specifying the spatial discretization scheme, we make the two following assumptions:

Assumption 5 (Pressure reconstructions)

There exist two scalar functions $s_{1,h\tau}$, $s_{2,h\tau}$, *continuous and piecewise affine in time and satisfying* $s_{1,h}^n := s_{1,h\tau}(\cdot,t^n) \in H_0^1(\Omega)$, $s_{2,h}^n := s_{2,h\tau}(\cdot,t^n) \in H_0^1(\Omega)$. *We call* $s_{1,h\tau}$, $s_{2,h\tau}$ pressure reconstructions.

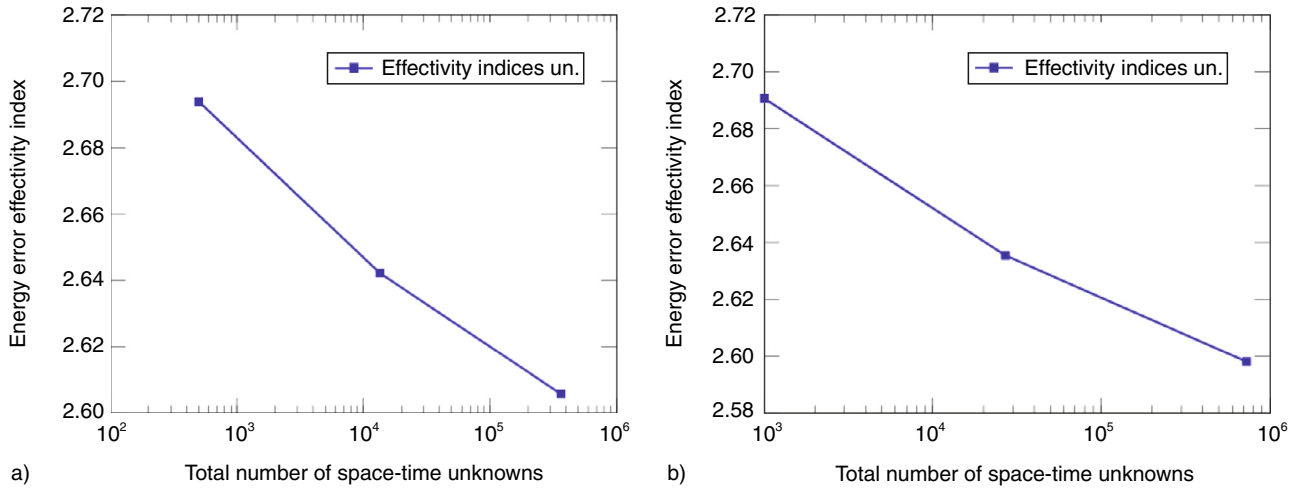

Figure 12

Effectivity indices for final times a) $t_F = 1.5$ and b) $t_F = 3$, energy norm error $||u - u_{h\tau}||_X$, single-phase unsteady Darcy flow.

Remark 3 (Assumption 5)

In a proper mathematical formulation of the two-phase flow model [83] there are two quantities which possess the same continuity as the weak potential in (26): these are the global pressure and the complementary pressure (Kirchhoff transform). For nonconforming discretizations, where the discrete versions of these quantities are not continuous, the scalar functions $s_{1,h\tau}$, $s_{2,h\tau}$ represent their continuous (in the sense of traces) reconstructions. Alternatively, when one knows for instance that the two phase pressures P_p, $p \in \mathcal{P}$, should physically be continuous, then $s_{1,h\tau}$, $s_{2,h\tau}$ may represent their reconstructions.

Assumption 6 (Equilibrated phase flux reconstructions)

There exist two vector functions $\boldsymbol{\sigma}_{p,h\tau}$, $p \in \mathcal{P}$, *piecewise constant in time, such that, for all* $1 \leq n \leq N$, $\boldsymbol{\sigma}^n_{p,h} := \boldsymbol{\sigma}_{p,h\tau}|_{I_n} \in \mathbf{H}(\mathrm{div}, \Omega)$, $p \in \mathcal{P}$, verifying:

$$(q^n_p - \partial_t(\phi S^n_{p,h\tau}) - \nabla \cdot \boldsymbol{\sigma}^n_{p,h}, 1)_T = 0 \quad \forall T \in \mathcal{T}^n_h$$

We call $\boldsymbol{\sigma}_{p,h\tau}$, $p \in \mathcal{P}$, *equilibrated phase flux reconstructions.*

For the following result, we suppose that we are on a certain time step t^n, $1 \leq n \leq N$, that some iterative linearization (*e.g.*, the Newton one) has been applied to the system of nonlinear algebraic equations resulting from the given numerical method and that we are on its step k, and that in order to solve the arising system of linear equations, some iterative linear solver has been applied, with the current step i. The corresponding saturation-pressure approximation couple on the time interval I_n is denoted by $(S^{n,k,i}_{p,h\tau}, P^{n,k,i}_{p,h\tau})$.

Theorem 3 (*A posteriori* error estimate, two-phase flow)

Let (S_p, P_p) *for one chosen* $p \in \mathcal{P}$ *be the exact (weak) saturation and pressure. Let* $(S_{p,h\tau}, P_{p,h\tau})$ *be their arbitrary piecewise regular in space and continuous and piecewise affine in time approximations. Let Assumptions 5 and 6 be satisfied. Let a time step* t^n, $1 \leq n \leq N$, *a linearization step* $k \geq 1$, *and an algebraic solver step* $i \geq 1$ *be given. Then:*

$$|||(S_p - S^{n,k,i}_{p,h\tau}, P_p - P^{n,k,i}_{p,h\tau})|||_{I_n} \leq \eta^{n,k,i}_{\mathrm{sp}} + \eta^{n,k,i}_{\mathrm{tm}} + \eta^{n,k,i}_{\mathrm{lin}} + \eta^{n,k,i}_{\mathrm{alg}} \tag{31}$$

where $\eta^{n,k,i}_{\mathrm{sp}}$, $\eta^{n,k,i}_{\mathrm{tm}}$, $\eta^{n,k,i}_{\mathrm{lin}}$, *and* $\eta^{n,k,i}_{\mathrm{alg}}$ *are respectively the spatial, temporal, linearization, and algebraic error estimators.*

The precise form of the error measure $|||\cdot|||_{I_n}$, as well as of the error estimators $\eta^{n,k,i}_{\mathrm{sp}}$, $\eta^{n,k,i}_{\mathrm{tm}}$, $\eta^{n,k,i}_{\mathrm{lin}}$, $\eta^{n,k,i}_{\mathrm{alg}}$, in particular for the different discretization schemes of Section 2, can be found in [83, 93].

3.4.2 Adaptivity: Stopping the Linear and Nonlinear Solvers and (De)refining the Mesh and Time Step

Theorem 3 enables to control the overall error in a numerical approximation of the two-phase flow problem. In addition to Sections 3.2 and 3.3, however, it allows to identify the different error components in the spirit of property (vi) from Section 3.1. It is thus suitable for designing an entirely adaptive algorithm, with adaptive stopping criteria for both linear and nonlinear solvers, adaptive time step choice, and adaptive mesh refinement and derefinement. We now illustrate numerically such adaptive procedures.

We consider an immiscible incompressible two-phase flow test case taken from [112], with $\mathcal{P} := \{\mathrm{w}, \mathrm{n}\}$. We neglect the gravity terms, use the Brooks–Corey relations, define the computational domain $\Omega = (0, 300)\,\mathrm{m} \times (0, 300)\,\mathrm{m}$, the final time $t_\mathrm{F} = 4 \times 10^6\,\mathrm{s}$, the porosity $\phi = 0.2$, the permeability tensor $\mathbf{K} = 10^{-11}\,\mathbb{I}\,\mathrm{m}^2$, the sources $q_\mathrm{w} = q_\mathrm{n} = 0\,\mathrm{s}^{-1}$, and the viscosities $\mu_\mathrm{w} = 5 \times 10^{-4}\ \mathrm{kg.m^{-1}.s^{-1}}$ and $\mu_\mathrm{n} = 2 \times 10^{-3}\,\mathrm{kg.m^{-1}.s^{-1}}$. The wetting and nonwetting residual saturations s_rw and s_rn from the Brooks–Corey model are both set equal to zero, whereas the entry pressure is taken as $p_\mathrm{d} = 5 \times 10^3\,\mathrm{kg.m^{-1}.s^{-2}}$. The initial wetting saturation is taken as $s_\mathrm{w}^0 = 0.2$ everywhere except of the lower left (injection) corner of Ω, where we set $s_\mathrm{w}^0 = 0.95$. A flow gradient is imposed by setting the Dirichlet boundary conditions as 0.95 and $3.45 \times 10^6\,\mathrm{kg.m^{-1}.s^{-2}}$ in the lower left corner and to 0.2 and $2.41 \times 10^6\,\mathrm{kg.m^{-1}.s^{-2}}$ in the upper right corner, for the wetting saturation and pressure respectively; elsewhere homogeneous Neumann boundary condition are considered. We consider a cell-centered TPFV space discretization, fully implicit time discretization, the Newton method for the linearization, and the Generalized Minimal Residual (GMRes) algebraic solver with Jacobi (diagonal) preconditioning for the arising systems of linear equations. All the examples are taken from [93], where all the details can be found.

In Figure 13a, for a fixed discrete time and Newton step, we track the dependence of the different estimators of Theorem 3 on the GMRes iterations. We see that all $\eta_\mathrm{sp}^{n,k,i}$, $\eta_\mathrm{tm}^{n,k,i}$, and $\eta_\mathrm{lin}^{n,k,i}$ stabilize after a few GMRes iterations, whereas $\eta_\mathrm{alg}^{n,k,i}$ as expected decreases with GMRes iterations. Classically, one would wait until the algebraic relative residual becomes very small, say smaller than 10^{-13}. In the present case, this requires 1 530 GMRes iterations. Our adaptive stopping criterion instead says that it is sufficient that the algebraic error estimate $\eta_\mathrm{alg}^{n,k,i}$ is some user-given constant γ_alg smaller than the sum $\eta_\mathrm{sp}^{n,k,i} + \eta_\mathrm{tm}^{n,k,i} + \eta_\mathrm{lin}^{n,k,i}$, expressing that there is no need to continue with algebraic solver iterations once the algebraic error does not influence the overall error significantly. For $\gamma_\mathrm{alg} = 10^{-3}$, such a criterion only requires 435 GMRes iterations. In Figure 13b, we then plot the different estimators as function of the Newton iterations, at the same discrete time. 11 iterations are necessary to reach the classical stopping criterion requiring the L^∞ difference (with appropriate weighting) between two consecutive pressure and saturation approximations to be smaller or equal to 10^{-11}, whereas only 3 iterations are sufficient to arrive at the adaptive stopping criterion $\eta_\mathrm{lin}^{n,k,i} \le \gamma_\mathrm{lin}(\eta_\mathrm{sp}^{n,k,i} + \eta_\mathrm{tm}^{n,k,i})$ with $\gamma_\mathrm{lin} = 10^{-3}$.

The overall gains achievable thanks to our approach are then illustrated in Figure 14. In Figure 14a, we plot the number of necessary Newton iterations on each time step for both the adaptive and classical stopping criteria. We can see that they are considerably smaller in the adaptive case. It is to be emphasized that in particular much fewer Jacobian matrix assemblies are necessary in our approach. In Figure 14b, the cumulative number of GMRes iterations is given as function of time. From this last graph, we can conclude that in the adaptive approach the number of cumulative GMRes iterations is approximately 12-times smaller compared to that in the classical one.

The above usage of *a posteriori* error estimates seems to be rather new. More common is the procedure already described in Section 3.3.2, consisting in equilibration of $\eta_\mathrm{sp}^{n,k,i}$ with $\eta_\mathrm{tm}^{n,k,i}$ and in equilibration of the individual element components $\eta_{\mathrm{sp},T}^{n,k,i}$ of $\eta_\mathrm{sp}^{n,k,i}$ through adaptive time

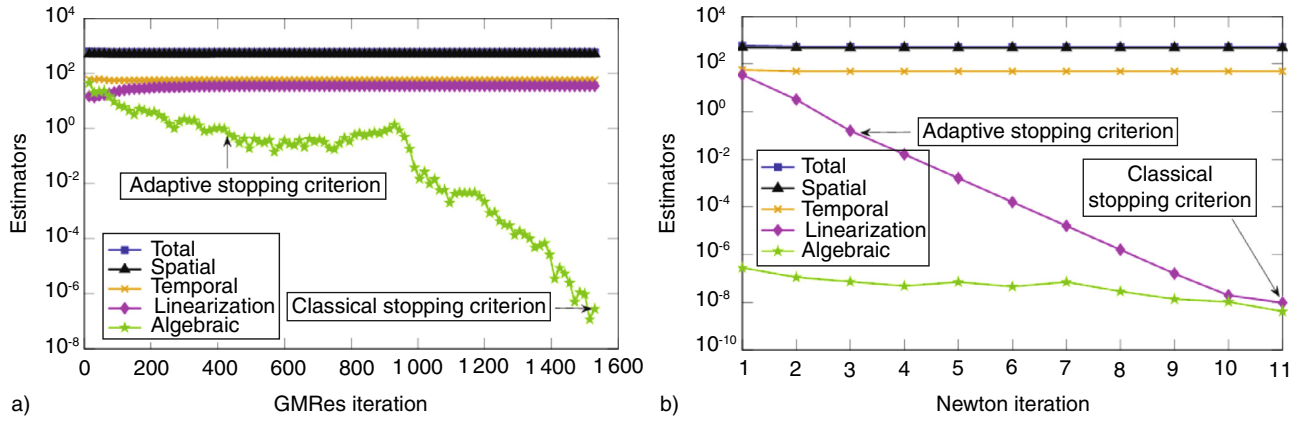

Figure 13

Spatial, temporal, linearization, and algebraic estimators and their sum as function of the GMRes iterations on the first Newton iteration a) and of the Newton iterations b) at time 2.6×10^6 s, two-phase Darcy flow. The pictures are taken from reference [93].

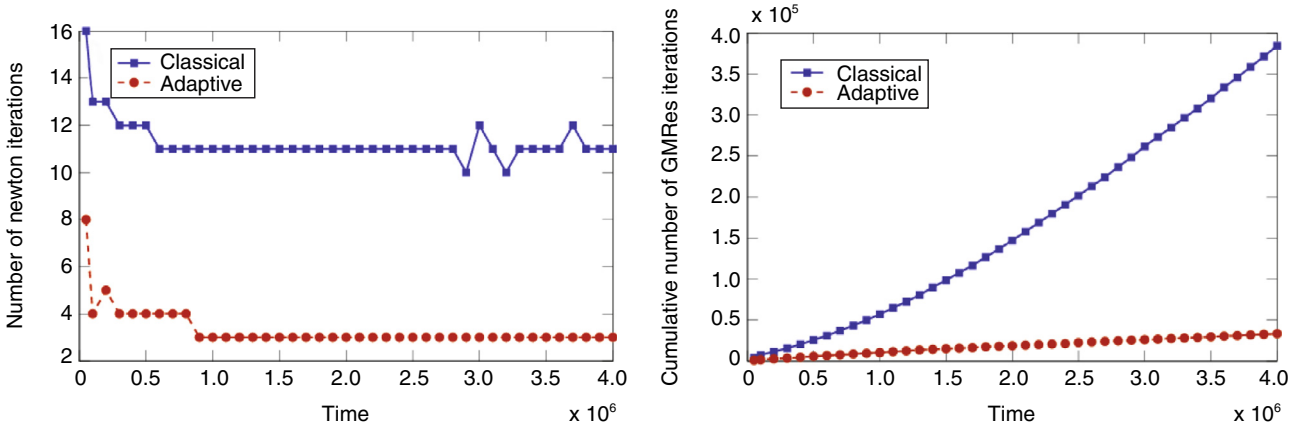

Figure 14

a) Number of Newton iterations on each time step and b) cumulative number of GMRes iterations as a function of time, two-phase Darcy flow. The pictures are taken from reference [93].

and space mesh refinement and derefinement. Adaptive algorithms and numerical experiments in such a spirit are presented in [93]. A simplified example can be summarized as follows:

Algorithm 1 (An entirely adaptive algorithm)

1. *Assembly the initial conditions. Set $n = 1$;*
2. *Set up the system of nonlinear algebraic equations on time t^n;*
3. (a) *Initialize the iterative linearization (typically by the last available approximations). Set $k = 1$;*
   (b) *Set up the system of linear algebraic equations on linearization step k;*
   (c) i. *Initialize the iterative linear solver (typically by the last available approximations). Set $i = 1$;*
   ii. *Perform one or several linear solver steps (in the latter case increase i appropriately). This gives the approximation $(S_{p,h\tau}^{n,k,i}, P_{p,h\tau}^{n,k,i})$;*
   iii. *From the numerical method at hand, build the pressure reconstructions $s_{1,h\tau}, s_{2,h\tau}$ and the equilibrated phase flux reconstructions $\boldsymbol{\sigma}_{p,h\tau}$, $p \in \mathcal{P}$;*
   iv. *Evaluate the estimators $\eta_{\text{sp}}^{n,k,i}$, $\eta_{\text{tm}}^{n,k,i}$, $\eta_{\text{lin}}^{n,k,i}$, $\eta_{\text{alg}}^{n,k,i}$;*
   v. *Check the convergence criterion for the linear solver:*

$$\eta_{\text{alg}}^{n,k,i} \leq \gamma_{\text{alg}} \left(\eta_{\text{sp}}^{n,k,i} + \eta_{\text{tm}}^{n,k,i} + \eta_{\text{lin}}^{n,k,i} \right) \tag{32}$$

If this criterion is not satisfied, increase i and go back to step 3(c)ii;

   (d) *Check the convergence criterion for the nonlinear solver:*

$$\eta_{\text{lin}}^{n,k,i} \leq \gamma_{\text{lin}} \left(\eta_{\text{sp}}^{n,k,i} + \eta_{\text{tm}}^{n,k,i} \right) \tag{33}$$

If this criterion is not satisfied, set $k := k + 1$ and go back to step 3b;

4. *Check whether the spatial and temporal errors are comparable in the sense that:*

$$\eta_{\text{sp}}^{n,k,i} \approx \eta_{\text{tm}}^{n,k,i} \tag{34}$$

whether the spatial errors are equally distributed in the computational domain in the sense that:

$$\eta_{\text{sp},T}^{n,k,i} \text{ are comparable for all } T \in \mathcal{T}_h^n \tag{35}$$

and whether the total error is small enough in the sense that:

$$\eta_{\text{sp}}^{n,k,i} + \eta_{\text{tm}}^{n,k,i} + \eta_{\text{lin}}^{n,k,i} + \eta_{\text{alg}}^{n,k,i} \leq \varepsilon^n \tag{36}$$

where ε^n is a user-given precision for the maximal error on the time interval I_n. If this is the case, and $t^n < t_{\text{F}}$, set $n := n + 1$ and go to step 2. If not, refine the time step τ^n and/or the space mesh $\mathcal{T}_h^n$ and go to step 2.

Remark 4 (Computational cost)

The above algorithm is essentially a very standard resolution algorithm. Its basic novel ingredients are the estimators $\eta_{\text{sp}}^{n,k,i}$, $\eta_{\text{tm}}^{n,k,i}$, $\eta_{\text{lin}}^{n,k,i}$, $\eta_{\text{alg}}^{n,k,\text{i}}$; according to property (v) of Section 3.1, their evaluation price is very small. The simplest adaptivity to implement in an existing program is then that of the adaptive stopping criteria (32) and (33). This basically consists in replacing two source code lines. It is more demanding to implement (34), (35), and (36).

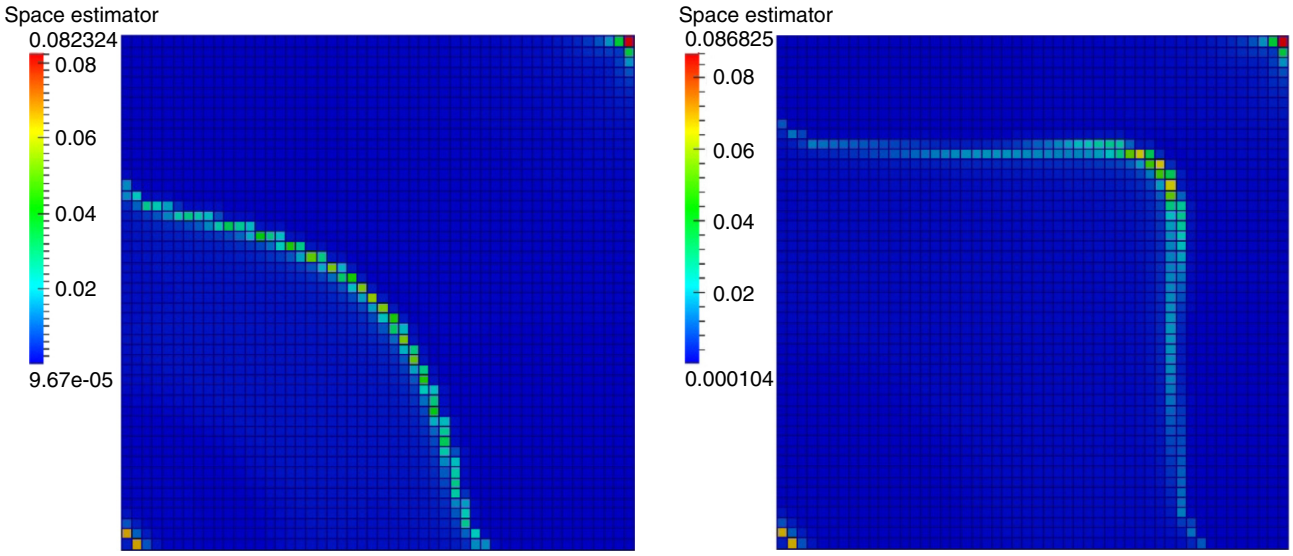

Figure 15

Spatial error distribution at time 6.8×10^7 s and 1.3×10^8 s, compositional multi-phase Darcy flow.

3.5 Compositional Unsteady Darcy Flow

We finally return back to the compositional multi-phase Darcy model introduced in Section 1. We recently in [113] adapted the developments presented in Section 3.4 for two-phase flows to this setting.

In [113], we have in particular derived an equivalent of Theorem 3 for the compositional multi-phase flow. Thus the overall error can be controlled and moreover its individual components identified. Similarly to Section 3.4.2, entirely adaptive algorithms were proposed for the compositional multi-phase flow case [113]. Results similar to those reported in Figures 13 and 14 were obtained, enabling in particular substantial computational gains just by employing adaptive stopping criteria for linear and nonlinear solvers. To illustrate the capability of our estimators to detect likewise the distribution of the spatial error, typically concentrated around the moving saturation front, we plot in Figure 15 the element contributions of the spatial estimator $\eta_{\mathrm{sp}}^{n,k,i}$ at two different discrete times. Refining and derefining the mesh adaptively while following the front (and choosing adaptively the time step size) is likely to still increase the computational attractiveness of our approach. One example of a simpler model problem with similar numerical difficulties for which an entirely adaptive algorithm has already been successfully put in place is discussed in [84].

ACKNOWLEDGMENTS

This work was partially supported by the ERT project "Enhanced oil recovery and geological sequestration of CO_2: mesh adaptivity, *a posteriori* error control, and other advanced techniques" (Université Pierre et Marie Curie/Laboratoire Jacques-Louis Lions and IFP Energies nouvelles).

REFERENCES

1 Coats K.H., Thomas L.K., Pierson R.G. (1998) Compositional and black oil reservoir simulation, *SPE Reservoir Evaluation and Engineering* **1**, 50990.

2 Chainais-Hillairet C., Enchéry G., Mamaghani M. (2011) Development of a refinement criterion for adaptive mesh refinement in steam-assisted gravity drainage simulation, *Comput. Geosci.* **15**, 1, 17-34.

3 Ding D., Jeannin L. (2001) A new methodology for singularity modelling in flow simulations in reservoir engineering, *Comput. Geosci.* **5**, 93-119.

4 Agélas L., Di Pietro D.A., Masson R. (2008) A symmetric and coercive finite volume scheme for multiphase porous media flow with applications in the oil industry, in Eymard R., Hérard J.-M. (eds), *Finite Volumes for Complex Applications V*, pp. 35-52, John Wiley & Sons, ISBN 978-1-84821-035-6.

5 Zienkiewicz O.C., Taylor R.L. (2000) *The finite element method*, volume 1 (The Basis), Butterworth-Heinemann, Oxford, 5th edition.

6 Eymard R., Gallouët T., Herbin R. (2010) Discretization of heterogeneous and anisotropic diffusion problems on general nonconforming meshes. SUSHI: a scheme using stabilization and hybrid interfaces, *IMA J. Numer. Anal.* **30**, 4, 1009-1043.

7 Di Pietro D.A., Ern A., Guermond J.-L. (2008) Discontinuous Galerkin methods for anisotropic semi-definite diffusion with advection, *SIAM J. Numer. Anal.* **46**, 2, 805-831.

8 Michel A. (2001) Convergence de schémas volumes finis pour des problèmes de convection diffusion non linéaires, *PhD Thesis*, Université de Provence.

9 Gallouët T., Larcher A., Latché J.C. (2012) Convergence of a finite volume scheme for the convection-diffusion equation with L^1 data, *Math. Comp.* **81**, 279, 1429-1454.

10 Andreianov B., Bendahmane M., Karlsen K.H. (2010) Discrete duality finite volume schemes for doubly nonlinear degenerate hyperbolic-parabolic equations, *J. Hyperbolic Diff. Equ.* **7**, 1, 1-67.

11 Cancès C., Cathala M., Le Potier C. (2013) Monotone corrections for generic cell-centered finite volume approximations of anisotropic diffusion equations, *Numer. Math.* **125**, 387–417.

12 Falgout R.D., Yang U.M. (2002) Hypre: a library of high performance preconditioners, in *Preconditioners, Lecture Notes in Computer Science*, 632-641.

13 Scheichl R., Vassilevski P.S., Zikatanov L.T. (2012) Mutilevel methods for elliptic problems with highly varying coefficients on non-aligned coarse grids, *SIAM J. Numer. Anal.* **50**, 3, 1675-1694.

14 Havé P., Masson R., Nataf F., Szydlarski M., Zhao T. (2013) Algebraic domain decomposition methods for highly heterogeneous problems, SIAM J. Sci. Comput. **35**, 3, C284-C302.

15 Efendiev Y., Galvis J., Ki Kang S., Lazarov R.D. (2012) Robust multiscale iterative solvers for nonlinear flows in highly heterogeneous media, *Numer. Math. Theory Methods Appl.* **5**, 3, 359-383.

16 Ayuso de Dios B., Zikatanov L. (2009) Uniformly convergent iterative methods for discontinuous Galerkin discretizations, *J. Sci. Comput.* **40**, 4-36.

17 Vohralík M., Wohlmuth B.I. (2013) Mixed finite element methods: implementation with one unknown per element, local flux expressions, positivity, polygonal meshes, and relations to other methods, *Math. Models Methods Appl. Sci.* **23**, 5, 803-838.

18 Di Pietro D.A. (2013) On the conservativity of cell centered Galerkin methods, *C. R. Acad. Sci. Paris, Ser. I* **351**, 155-159.

19 Di Pietro D.A., Lemaire S. (2013) An extension of the Crouzeix-Raviart space to general meshes with application to quasi-incompressible linear elasticity and Stokes flow, Math. Comp. Accepted for publication. *Preprint* http://hal.archives-ovverter.fr/hal/00611997

20 Kim K.Y. (2007) *A posteriori* error estimators for locally conservative methods of nonlinear elliptic problems, *Appl. Numer. Math.* **57**, 9, 1065-1080.

21 Ern A., Nicaise S., Vohralík M. (2007) An accurate H(div) flux reconstruction for discontinuous Galerkin approximations of elliptic problems, *C. R. Math. Acad. Sci. Paris* **345**, 12, 709-712.

22 Di Pietro D.A., Ern A. (2011) *Mathematical aspects of discontinuous Galerkin methods,* volume 69 of *Mathématiques & Applications*, Springer-Verlag, Berlin.

23 Ainsworth M., Oden J.T. (2000) *A posteriori error estimation in finite element analysis*. Pure and Applied Mathematics (New York), Wiley-Interscience, John Wiley & Sons, New York, ISBN 0-471-29411-X.

24 Destuynder P., Métivet B. (1999) Explicit error bounds in a conforming finite element method, *Math. Comp.*, **68**, 228, 1379-1396.

25 Luce R., Wohlmuth B.I. (2004) A local *a posteriori* error estimator based on equilibrated fluxes, *SIAM J. Numer. Anal.*, **42**, 4, 1394-1414.

26 Braess D., Schöberl J. (2008) Equilibrated residual error estimator for edge elements, *Math. Comp.* **77**, 262, 651-672.

27 Ern A., Vohralík M. (2013) Adaptive inexact Newton methods with *a posteriori* stopping criteria for nonlinear diffusion PDEs, *SIAM J. Sci. Comput.* **35**, 4, A1761-A1791.

28 Di Pietro D.A., Gratien J.-M. (2011) Lowest order methods for diffusive problems on general meshes: a unified approach to definition and implementation, in *Finite Volumes for Complex Applications VI Problems & Perspectives*, Prague, Springer-Verlag, Vol. **2**, pp. 3-19.

29 Di Pietro D.A., Gratien J.-M., Prud'homme C. (2013) A domain-specific embedded language in C++ for lowest-order discretizations of diffusive problems on general meshes, *BIT Numerical Mathematics* **53**, 1, 111-152.

30 Grospellier G., Lelandais B. (2009) The Arcane development framework, *Proceedings of the 8th workshop on Parallel/High-Performance Object-Oriented Scientific Computing* POOSC '09, pp. 4:1-4:11, New York, NY, USA, ACM.

31 Prud'homme C., Chabannes V., Doyeux V., Ismail M., Samake A., Peña G. (2012) Feel++: a computational framework for Galerkin methods and advanced numerical methods, Coquel F., Gutnic M., Helluy P., Lagoutière F., Rohde C., Seguin N., *ESAIM: Proceedings*, Vol. **38**, pp. 429-455.

32 Flemisch B., Darcis M., Erbertseder K., Faigle B., Lauser A., Mosthaf K., Müthing S., Nuske P., Tatomir A., Wolff M., Helmig R. (2011) DuMu: DUNE for multi-Phase, Component, Scale, Physics,... Flow and transport in porous media, *Adv. Water Res.* **34**, 9, 1102-1112.

33 Bassi F., Botti L., Colombo A., Di Pietro D.A., Tesini P. (2012) On the flexibility of agglomeration based physical space discontinuous Galerkin discretizations, *J. Comput. Phys.* **231**, 1, 45-65.

34 Aavatsmark I., Barkve T., Bøe Ø., Mannseth T. (1994) Discretization on non-orthogonal, curvilinear grids for multi-phase flow, *Proc. of the 4th European Conf. on the Mathematics of Oil Recovery*, volume D, Røros, Norway.

35 Edwards M.G., Rogers C.F. (1994) A flux continuous scheme for the full tensor pressure equation, in *Proc. of the 4th European Conf. on the Mathematics of Oil Recovery*, volume D, Røros, Norway.

36 Agélas L., Di Pietro D.A., Droniou J. (2010) The G method for heterogeneous anisotropic diffusion on general meshes, *M2AN Math. Model. Numer. Anal.* **44**, 4, 597-625.

37 Aavatsmark I., Eigestad G.T., Mallison B.T., Nordbotten J.M. (2008) A compact multipoint flux approximation method with improved robustness, *Numer. Methods Partial Differential Equations* **24**, 5, 1329-1360.

38 Aavatsmark I. (2002) An introduction to multipoint flux approximations for quadrilateral grids, *Comput. Geosci.* **6**, 3-4, 405–432.

39 Agélas L., Masson R. (2008) Convergence of the finite volume MPFA O scheme for heterogeneous anisotropic diffusion problems on general meshes, *C. R. Acad. Sci. Paris, Ser. I* **346**, 1007-1012.

40 Di Pietro D.A. (2012) Cell centered Galerkin methods for diffusive problems, *M2AN Math. Model. Numer. Anal.* **46**, 1, 111-144.

41 Vohralík M. (2006) Equivalence between lowest-order mixed finite element and multi-point finite volume methods on simplicial meshes, *M2AN Math. Model. Numer. Anal.* **40**, 2, 367-391.

42 Raviart P.-A., Thomas J.-M. (1977) A mixed finite element method for 2nd order elliptic problems, in *Mathematical aspects of finite element methods (Proc. Conf., Consiglio Naz. delle Ricerche (C.N.R.), Rome, 1975)*, pp. 292-315. Lecture Notes in Math., Vol. **606**, Springer, Berlin.

43 Brezzi F., Fortin M. (1991) *Mixed and hybrid finite element methods*, Vol. **15** *Springer Series in Computational Mathematics*, Springer-Verlag, New York, ISBN 0387-97582-9.

44 Younès A., Mosé R., Ackerer P., Chavent G. (1999) A new formulation of the mixed finite element method for solving elliptic and parabolic PDE with triangular elements, *J. Comput. Phys.* **149**, 1, 148-167.

45 Hoffmann J. (2008) Equivalence of the lowest-order Raviart–Thomas mixed finite element method and the multi point flux approximation scheme on triangular grids. Preprint, University of Erlangen-Nürnberg.

46 Younès A., Fontaine V. (2008) Hybrid and multi-point formulations of the lowest-order mixed methods for Darcy's flow on triangles, *Internat. J. Numer. Methods Fluids* **58**, 9, 1041-1062.

47 Brezzi F., Lipnikov K., Shashkov M. (2005) Convergence of the mimetic finite difference method for diffusion problems on polyhedral meshes, *SIAM J. Numer. Anal.* **43**, 5, 1872-1896.

48 Brezzi F., Lipnikov K., Simoncini V. (2005) A family of mimetic finite difference methods on polygonal and polyhedral meshes, *Math. Models Methods Appl. Sci.* **15**, 10, 1533-1551.

49 Brezzi F., Lipnikov K., Shashkov M. (2006) Convergence of mimetic finite difference methods for diffusion problems on polyhedral meshes with curved faces, *Math. Models Methods Appl. Sci.* **16**, 2, 275-298.

50 Eymard R., Gallouët T., Herbin R. (2007) A new finite volume scheme for anisotropic diffusion problems on general grids: convergence analysis, *C. R. Acad. Sci. Paris, Ser. I* **344**, 403-406.

51 Droniou J., Eymard R. (2006) A mixed finite volume scheme for anisotropic diffusion problems on any grid, *Numer. Math.* **105**, 1, 35-71.

52 Di Pietro D.A. (2010) Cell centered Galerkin methods, *C. R. Acad. Sci. Paris, Ser. I* **348**, 31-34.

53 Droniou J., Eymard R., Gallouët T., Herbin R. (2010) A unified approach to mimetic finite difference, hybrid finite volume and mixed finite volume methods, *Math. Models Methods Appl. Sci.* **20**, 2, 265-295.

54 Droniou J., Eymard R., Gallouët T., Herbin R. (2013) Gradient schemes: a generic framework for the discretisation of linear, nonlinear and nonlocal elliptic and parabolic equations, *Math. Models Meth. Appl. Sci.* **12**, 13-15.

55 Bonelle J., Ern A. (2014) Analysis of compatible discrete operator schemes for elliptic problems on polyhedral meshes, *M2AN Math. Model. Numer. Anal.* **48**, 2, 553-581.

56 Droniou J. (2013) Finite volume schemes for diffusion equations: introduction to and review of modern methods, *Math. Models Meth. Appl. Sci.* Accepted for publication.

57 Allaire G. (2009) *Analyse numérique et optimisation*, Les éditions de l'École Polytechnique, Palaiseau, France.

58 Di Pietro D.A., Ern A. (2010) Discrete functional analysis tools for discontinuous Galerkin methods with application to the incompressible Navier-Stokes equations, *Math. Comp.* **79**, 1303-1330.

59 Arnold D.N. (1982) An interior penalty finite element method with discontinuous elements, *SIAM J. Numer. Anal.* **19**, 742-760.

60 Brenner S.C. (2003) Poincaré-Friedrichs inequalities for piecewise H^1 functions, *SIAM J. Numer. Anal.* **41**, 1, 306-324.

61 Burman E., Zunino P. (2006) A domain decomposition method for partial differential equations with non-negative form based on interior penalties, *SIAM J. Numer. Anal.* **44**, 1612-1638.

62 Reed W.H., Hill T.R. (1973) Triangular mesh methods for the neutron transport equation. Technical Report LA-UR-73-0479, http://lib-www.lanl.gov/cgi-bin/getfile?00354107.pdf, Los Alamos Scientific Laboratory, Los Alamos, NM.

63 Lesaint P. (1973) Finite element methods for symmetric hyperbolic equations, *Numer. Math.* **21**, 244-255.

64 Lesaint P. (1975) Sur la résolution des systèmes hyperboliques du premier ordre par des méthodes d'éléments finis, *PhD Thesis*, Université Pierre et Marie Curie (Paris 6).

65 Lesaint P., Raviart P.-A. (1974) On a finite element method for solving the neutron transport equation, in *Mathematical Aspects of Finite Elements in Partial Differential Equations*, pp. 89-123. Publication No. 33. Math. Res. Center, Univ. of Wisconsin-Madison, Academic Press, New York.

66 Cockburn B., Shu C.-W. (1989) TVB Runge-Kutta local projection discontinuous Galerkin finite element method for conservation laws. II. General framework, *Math. Comp.* **52**, 186, 411-435.

67 Cockburn B., Shu C.-W. (1991) The Runge-Kutta local projection P^1-discontinuous-Galerkin finite element method for scalar conservation laws, *RAIRO Modél. Math. Anal. Numér.* **25**, 3, 337-361.

68 Nitsche J. (1971) Über ein Variationsprinzip zur Lösung von Dirichlet-Problemen bei Verwendung von Teilräumen, die keinen Randbedingungen unterworfen sind, *Abh. Math. Sem. Univ. Hamburg* **36**, 9-15. Collection of articles dedicated to Lothar Collatz on his sixtieth birthday.

69 Nitsche J. (1972) On Dirichlet problems using subspaces with nearly zero boundary conditions, *The mathematical foundations of the finite element method with applications to partial differential equations (Proc. Sympos., Univ. Maryland, Baltimore, Md., 1972)*, Academic Press, New York, pp. 603-627.

70 Babuška I. (1973) The finite element method with penalty, *Math. Comp.* **27**, 221-228.

71 Baker G.A. (1977) Finite element methods for elliptic equations using nonconforming elements, *Math. Comp.* **31**, 137, 45-49.

72 Wheeler M.F. (1978) An elliptic collocation-finite element method with interior penalties, *SIAM J. Numer. Anal.* **15**, 1, 152-161.

73 Bassi F., Rebay S. (1997) A high-order accurate discontinuous finite element method for the numerical solution of the compressible Navier-Stokes equations, *J. Comput. Phys.* **131**, 2, 267-279.

74 Arnold D.N., Brezzi F., Cockburn B., Marini L.D. (2002) Unified analysis of discontinuous Galerkin methods for elliptic problems, *SIAM J. Numer. Anal.* **39**, 5, 1749-1779.

75 Ern A., Guermond J.-L. (2006) Discontinuous Galerkin methods for Friedrichs' systems. I. General theory, *SIAM J. Numer. Anal.* **44**, 2, 753-778.

76 Ern A., Guermond J.-L. (2006) Discontinuous Galerkin methods for Friedrichs' systems. II. Second-order elliptic PDEs, *SIAM J. Numer. Anal.* **44**, 6, 2363-2388.

77 Ern A., Guermond J.-L. (2008) Discontinuous Galerkin methods for Friedrichs' systems. III. Multi-field theories with partial coercivity, *SIAM J. Numer. Anal.* **46**, 2, 776-804.

78 Sun D.C., Wheeler M.F. (2005) L2(H1) norm *a posteriori* error estimation for discontinuous Galerkin approximations of reactive transport problems, *J. Sci. Comp.* **205**, 501-530.

79 Sun D.C., Wheeler M.F. (2005) Discontinuous Galerkin methods for coupled flow and reactive transport problems, *Appl. Numer. Math.* **52**, 2-3, 283-298.

80 Bastian P., Engwer C., Fahlke J., Ippisch O. (2011) An unfitted discontinuous Galerkin method for pore-scale simulations of solute transport, *Math. Comput. Simul.* **81**, 10, 2051-2061.

81 Houston P., Schwab C., Süli E. (2002) Discontinuous hp-finite element methods for advection-diffusion-reaction problems, *SIAM J. Numer. Anal.* **39**, 2133-2163.

82 Scovazzi G., Gerstenberger A., Collis S.S. (2014) A discontinuous Galerkin method for gravity-driven viscous fingering instabilities in porous media, *J. Comput. Phys.* **233**, 373-399.

83 Cancès C., Pop I.S., Vohralík M. (2014) An *a posteriori* error estimate for vertex-centered finite volume discretizations of immiscible incompressible two-phase flow, *Math. Comp.*, **83**, 153-188.

84 Di Pietro D.A., Vohralík M., Yousef S. (2012) Adaptive regularization, linearization, discretization, and *a posteriori* error control for the two-phase Stefan problem, *Math. Comp.* Accepted for publication.

85 El Alaoui L., Ern A., Vohralík M. (2011) Guaranteed and robust *a posteriori* error estimates and balancing discretization and linearization errors for monotone nonlinear problems, *Comput. Methods Appl. Mech. Engrg.* **200**, 37-40, 2782-2795.

86 Ern A., Vohralík M. (2010) *A posteriori* error estimation based on potential and flux reconstruction for the heat equation, *SIAM J. Numer. Anal.* **48**, 1, 198-223.

87 Ern A., Vohralík M. (2011) A unified framework for *a posteriori* error estimation in elliptic and parabolic problems with application to finite volumes, in Fořt J., Fürst J., Halama J., Herbin R., Hubert F. (eds), *Finite Volumes for Complex Applications VI*, pp. 821-837, Berlin, Heidelberg, Springer-Verlag. ISBN 978-3-642-20670-2.

88 Hannukainen A., Stenberg R., Vohralík M. (2012) A unified framework for *a posteriori* error estimation for the Stokes problem, *Numer. Math.* **122**, 4, 725-769.

89 Jiránek P., Strakoš Z., Vohralík M. (2010) *A posteriori* error estimates including algebraic error and stopping criteria for iterative solvers, *SIAM J. Sci. Comput.* **32**, 3, 1567-1590.

90 Vohralík M. (2008) Residual flux-based *a posteriori* error estimates for finite volume and related locally conservative methods, *Numer. Math.* **111**, 1, 121-158.

91 Vohralík M. (2011) Guaranteed and fully robust *a posteriori* error estimates for conforming discretizations of diffusion problems with discontinuous coefficients, *J. Sci. Comput.* **46**, 3, 397-438.

92 Vohralík M. (2012) *A posteriori error estimates for efficiency and error control in numerical simulations*, Université Pierre et Marie Curie (Paris 6), Lecture notes, Course NM497.

93 Vohralík M., Wheeler M.F. (2013) *A posteriori* error estimates, stopping criteria, and adaptivity for two-phase flows. *Comput. Geosci.* **17**, 5, 789-812.

94 Prager W., Synge J.L. (1947) Approximations in elasticity based on the concept of function space, *Quart. Appl. Math.* **5**, 241-269.

95 Ladevèze P. (1975) Comparaison de modèles de milieux continus, *PhD Thesis*, Université Pierre et Marie Curie (Paris 6).

96 Verfürth R. (1996) *A review of a posteriori error estimation and adaptive mesh-refinement techniques*, Teubner-Wiley, Stuttgart. ISBN 3-519-02605-8.

97 Neittaanmäki P., Repin S. (2004) *Reliable methods for computer simulation,* volume 33 *of Studies in Mathematics and its Applications*, Elsevier Science B.V., Amsterdam. ISBN 0-444-51376-0. Error control and *a posteriori* estimates.

98 Repin S.I. (2008) *A posteriori estimates for partial differential equations*, volume 4 of *Radon Series on Computational and Applied Mathematics,* Walter de Gruyter GmbH & Co. KG, Berlin, ISBN 978-3-11-019153-0.

99 Babuška I., Rheinboldt W.C. (1978) Error estimates for adaptive finite element computations, *SIAM J. Numer. Anal.* **15**, 4, 736-754.

100 Ladevèze P., Leguillon D. (1983) Error estimate procedure in the finite element method and applications, *SIAM J. Numer. Anal.* **20**, 3, 485-509.

101 Carstensen C., Funken S.A. (1999) Fully reliable localized error control in the FEM, *SIAM J. Sci. Comput.* **21**, 4, 1465-1484.

102 Verfürth R. (2003) *A posteriori* error estimates for finite element discretizations of the heat equation, *Calcolo* **40**, 3, 195-212.

103 Ainsworth M. (2005) A synthesis of *a posteriori* error estimation techniques for conforming, non-conforming and discontinuous Galerkin finite element methods, in *Recent advances in adaptive computation*, Vol. **383**, Contemp. Math., 1-14. Amer. Math. Soc., Providence, RI.

104 Nicaise S. (2005) *A posteriori* error estimations of some cell-centered finite volume methods, *SIAM J. Numer. Anal.* **43**, 4, 1481-1503.

105 Vejchodský T. (2006) Guaranteed and locally computable *a posteriori* error estimate, *IMA J. Numer. Anal.* **26**, 3, 525-540.

106 Becker R., Johnson C., Rannacher R. (1995) Adaptive error control for multigrid finite element methods, *Computing* **55**, 4, 271-288.

107 Chaillou A.L., Suri M. (2006) Computable error estimators for the approximation of nonlinear problems by linearized models, *Comput. Methods Appl. Mech. Eng.* **196**, 1-3, 210-224.

108 Deuflhard P. (2004) *Newton methods for nonlinear problems*, volume 35 of *Springer Series in Computational Mathematics*, Springer-Verlag, Berlin, ISBN 3-540-21099-7. Affine invariance and adaptive algorithms.

109 Liesen J., Strakoš Z. (2013) *Krylov Subspace Methods. Principles and Analysis*, Numerical Mathematics and Scientific Computation. Oxford University Press, Oxford, United Kingdom, ISBN 978-0-19-965541-0.

110 Bernardi C., Verfürth R. (2000) Adaptive finite element methods for elliptic equations with non-smooth coefficients, *Numer. Math.* **85**, 4, 579-608.

111 Hilhorst D., Vohralík M. (2011) *A posteriori* error estimates for combined finite volume–finite element discretizations of reactive transport equations on nonmatching grids, *Comput. Methods Appl. Mech. Engrg.* **200**, 5-8, 597-613.

112 Klieber W., Rivière B. (2006) Adaptive simulations of two-phase flow by discontinuous Galerkin methods, *Comput. Methods Appl. Mech. Engrg.*, **196**, 1-3, 404-419.

113 Di Pietro D.A., Vohralík M., Yousef S. (2013) *A posteriori* error estimates, stopping criteria, and adaptivity for compositional multi-phase flows. Preprint HAL-00839487.

Manuscript accepted in May 2013
Published online in June 2014